

**ULTRASONOGRAPHIC EXAMINATION OF COWS AFFECTED WITH OVARIAN
FOLLICULAR DYSPLASIA**

by

Humberto de Castro e Nobre

A thesis submitted to the Graduate Faculty of
Auburn University
in partial fulfillment of the
requirements for the Degree of
Masters of Science

Auburn, Alabama
May 6, 2019

Keywords: Cattle, Ultrasonographic examination, Ovarian follicular dysplasia.

Copyright 2019 by Humberto de Castro e Nobre

Approved by

Julie Gard Schunelle Co-chair, Professor of Clinical Sciences
Misty Edmondson Co-chair, Associate State Veterinarian of Agriculture and Industries
James Wenzel, Professor Emeritus of Clinical Sciences
John Roberts, Clinical Lecturer of Pathobiology
Tim Braden, Associate Professor of Anatomy Physiology and Pharmacology
Ricardo Stockler, Assistant Clinical Professor of Clinical Sciences

ABSTRACT

A study commissioned by Florida Cattleman's Association in 2007, 2016 and 2017 found ovarian follicular dysplasia (OFD) to be the major abnormal ovarian condition linked to subfertility and infertility in Florida's beef herd. Ovarian follicular dysplasia is a slowly progressive bilateral abnormal growth and/or development of ovarian follicles that eventually transforms into "Sertoli-form" Granulosa Theca Cell Tumor (GTCT). The objective of this study was to determine the variation in ultrasound examination when compared to histologic findings utilizing 7MHz and 8MHz linear probes. Ante-mortem and post-mortem ultrasound images, magnetic resonance imaging and histology of 35 cows' ovaries were blindly compared for classification of different stages of OFD. Our hypothesis was that an 8MHz or greater ultrasound probe could be utilized for detection of earlier stages of OFD.

A comparison of all groups found that there was a 77.1% diagnostic agreement for presence of OFD between the ultrasound and histological analysis for OFD. The agreement of post-mortem ultrasonography with histologic examination for detection of OFD in groups 1 and 2 remained the same as the ante-mortem-histologic examination being 66.6% and 93.3%, respectively. The first group (group 1) was composed of 15 heifers, and the second group (group 2) was comprised of 15 cows. All animals from groups 1 and 2 were *Bos t. indicus* (Brahman) x *Bos t. taurus* (Angus, Simmental, Charolais). Most of the disagreement was found with calling an ovary OFD grade I that was histologically found to be normal, type I error. If the OFD grade I's were removed

from this analysis, then there would be 100% agreement between ultrasound and histology for diagnosis of OFD. The discrepancy between ultrasound grading and histological grading is based on a number of important factors such as amount of ovary evaluated, microscopic versus macroscopic (gross) analysis, and interpretation of what the hyperechogenicity represents. The ultrasound picture can be misleading because of the various angles and the density of the tissues is compounded throughout the ovary. However, some significant correlations were found when comparing the ultrasound versus the histological analysis.

Statistical analysis was performed and found that the p-value for testing correlation of histological follicle number (HFol) and ante-mortem ultrasound follicle number (AFol) was found to be less than 0.05, therefore the correlation between HFol and AFol was found to be statistically significant in group 1. The p-value for testing correlation of ante-mortem ultrasound hyperechogenicity grade (AHEch) and ante-mortem OFD grade (AOFD) was found to be less than 0.05, therefore the correlation between AHEch and AOFD was found to be statistically significant for group 2. The p-value for the testing correlation of ante-mortem ultrasound OFD grade (AOFD) and histologic OFD grade (HOFD) was found to be less than 0.05. Therefore, the correlation between AOFD and HOFD was statistically significant for group 2. The p-value for testing correlation of post-mortem ultrasound OFD grade (POFD) and histological OFD grade (HOFD) was found to be less than 0.05, therefore the correlation between POFD and HOFD was statistically significant for group 2. The p-value for testing correlation of

post-mortem hyperechogenicity score (PHEch) and post-mortem OFD score (POFD) was less than 0.05, therefore the correlation between PHEch and POFD was found to be statistically significant. The p-value for testing correlation of AHEch and post-mortem hyperechogenicity (PHEch) was not less than 0.05, therefore the correlation between AHEch and PHEch was not statistically significant for group 2. The p-value for testing correlation of AOFD and POFD was not less than 0.05. Therefore, the correlation between AOFD and POFD was not statistically significant

Also, one ovary from each animal in Groups 1, 2 and 3 was also submitted for MRI. The evaluation of the MRI images was inconclusive for the presence of OFD. After MRI was performed, five ovaries were submitted for CT in an effort to more accurately determine the presence of dystrophic mineralization within the ovary. The CT results showed that 20% of the ovaries contained some areas of mineralized tissue. Additional studies are necessary to determine the tissues that may lead to the hyperechoic areas within the ovary. More comparison studies are needed between histology, ultrasound, MRI and micro-CT to more fully elucidate the connection between histological analysis and ultrasound.

Furthermore, the difference between 7MHz (ante-mortem US) and 8MHz (post-mortem US) probes' did not affect the results of this study and both correlated with histological detection of OFD. This study also showed a correlation between ante-mortem and post-mortem US AFC and US HEch as well as a correlation between US AFT and MRI AFT. Trans-rectal ultrasound is a reliable tool to diagnose OFD ante-mortem.

ACKNOWLEDGMENTS

Thanks to the faculty and staff of the Auburn University College of Veterinary Medicine.

My sincere appreciation to my family and friends who always supported me during the completion of this project.

The guidance provided by Dr. Julie Gard in research design, scientific writing, professional presentations, friendship, patience, and especially the lessons of life are graciously acknowledged with the deepest of gratitude.

Thanks to Dr. Misty Edmondson and the Food Animal section for the opportunity to be part of the Auburn family, for the friendship, and all the advice that was given to me.

Thanks also to Dr. Tim Braden and Dr. John Roberts for allowing me work with them on this discovery in the field of Veterinary Medicine and their friendship.

Gratitude is also extended to Dr. James Wenzel and Dr. Ricardo Stockler for their support, words of encouragement, and for the friendship.

TABLE OF CONTENTS

ABSTRACT	ii
ACKNOWLEDGMENTS	v
LIST OF FIGURES	vii
LIST OF TABLES	xi
LIST OF APPENDICES	xii
LIST OF ABBREVIATIONS	xvi
I. INTRODUCTION	1
II. LITERATURE REVIEW	5
A. <u>Anatomical Structures</u>	5
B. <u>Embryogenesis</u>	6
C. <u>Sexual Differentiation</u>	8
D. <u>Oogenesis</u>	11
E. <u>Apoptosis</u>	17
F. <u>Paraovarian and Ovarian Cysts</u>	17
G. <u>Granulosa Theca Cell Tumor and Sertoli Cell Tumor</u>	19
H. <u>Ultrasonography</u>	21
III. JOURNAL ARTICLE	24
A. STATEMENT OF RESEARCH OBJECTIVES	24
B. MATERIAL AND METHODS	24
a. <u>Animals</u>	24
b. <u>Collection of Ultrasound Images</u>	25
c. <u>Collection of Magnetic Resonance Imaging and Computed Tomography</u>	30
d. <u>Histological Analysis</u>	31
e. <u>Statistical Analysis</u>	37
C. RESULTS	37
D. DISCUSSION	52
E. CONCLUSIONS	58
REFERENCES	60

LIST OF FIGURES

Figure 1. Reproductive tract samples collected for analysis and placed in labelled containers	27
Figure 2. Fixed ovaries being assembled into plastic pouches for post-mortem ultrasonographic examination.	29
Figure 3. Image of examination of post-mortem ovaries using the ultrasound machine Ibex EVO.	29
Figure 4. Fixed ovaries in plastic pouches grouped together for MRI examination.	31
Figure 5. Hematoxylin and eosin stained histologic section of an ovary with Grade I ovarian follicular dysplasia.	34
Figure 6. Hematoxylin and eosin stained histologic section of a normal ovary with primary, Graafian, and atretic follicles present within the ovarian stroma.	34
Figure 7. Hematoxylin and eosin stained histologic section of an ovary with grade II ovarian follicular dysplasia.	35
Figure 8. Hematoxylin and eosin stained histologic section of an ovary with grade III ovarian follicular dysplasia.	35
Figure 9. Hematoxylin and eosin stained histologic section of an ovary with grade III ovarian follicular dysplasia (OFD) with dystrophic mineralization (black arrows labelled M) and OFD cysts.	36
Figure 10. Hematoxylin and eosin stained histologic section of an ovary with grade IV ovarian follicular dysplasia.	36

Figure 11. Graph illustrating the ante-mortem average scores of US hyperechogenicity and US OFD grades of ovaries in group 1.	38
Figure 12. Graph illustrating the ante-mortem US hyperechogenicity scores and US OFD grades of ovaries in group 1.	39
Figure 13. Graph illustrating the ante-mortem average scores of US hyperechogenicity and US OFD grades of ovaries in group 2.	39
Figure 14. Graph illustrating the ante-mortem US hyperechogenicity scores and US OFD grades of ovaries in group 2.	40
Figure 15. Trans-rectal ultrasound image above is the right ovary taken ante-mortem. Multiple areas of hyperechogenicity are present in the ovary along with decreased numbers of Graffian follicles indicative of a grade IV OFD cow.	41
Figure 16. Trans-rectal ultrasound image of the left ovary taken ante-mortem. There are multiple areas of hyperechogenicity and small cystic areas indicative of a grade IV OFD cow.	42
Figure 17. Trans-rectal ultrasound image of the ovary of a cow with grade II OFD taken ante-mortem. There are early cystic follicles (red arrows) with small areas of hyperechogenicity in the echoic rim. The cow was diagnosed with grade II OFD via trans-rectal ultrasound and was confirmed via histological analysis.	43

Figure 18. Ultrasound image of a cow with grade II OFD. There is a corpus luteum (blue arrow) with small areas of hyperechogenicity. The cow was diagnosed with grade II OFD via ultrasound and was confirmed via histological analysis.	44
Figure 19. Graph illustrating the number of detected ovaries with OFD grades between ante-mortem US (AOFD) and histology (HOFD). Both methods of evaluation used 60 ovaries (from group 1 and 2).	46
Figure 20. Graph illustrating the number of detected ovaries with OFD grades between post-mortem US (POFD) and histology (HOFD). Both methods of evaluation used 30 ovaries (from group 1, 2 and 3).	46
Figure 21. Graph illustrating the presence of OFD between post-mortem US (POFD) and histologic (HOFD) analysis of five ovaries from group 3.	47
Figure 22. Ultrasound image of an ovary during MRI analysis. This ovary had OFD grade I via histology.	48
Figure 23. Image of MRI on five ovaries.	49
Figure 24. Graph illustrating the average numbers for antral follicle count (AFC) between post-mortem US and MRI evaluation of five ovaries from group 3.	50
Figure 25. Graph illustrating the total numbers for antral follicle count (AFC) between post-mortem US and MRI evaluation of five ovaries from group 3.	50
Figure 26. Three of the five ovaries evaluated via CT. The ovary located in the middle has two distinct mineralized areas. It was graded as OFD I via histology.	51

Figure 27. Graph illustrates the post-mortem US hyperechogenicity (HEch) degree of mineralization on CT and histologic OFD (HOFD) grade of ovaries from group 3.

51

LIST OF TABLES

TABLE 1. Ultrasonographic hyperechogenicity scoring system used in evaluation of the ultrasound images.	28
TABLE 2. Ultrasonographic OFD grading system applied to the ultrasound images.	28

LIST OF APPRNDICES

APPENDIX 1 - Graph illustrating the average of ante-mortem antral follicle count (AFC) number of small follicles (<4mm) in ovaries with US OFD grades I, II and III from group 1.	64
APPENDIX 2 - Graph illustrating the ante-mortem antral follicle count (AFC) numbers of small follicles (<4mm) in ovaries with US OFD grades I, II and III from group 1.	64
APPENDIX 3 - Graph illustrating the average of ante-mortem antral follicle count (AFC) numbers of large follicles (≥ 5 mm) in ovaries with US OFD grades I, II and III from group 1.	65
APPENDIX 4 - Graph illustrating the ante-mortem antral follicle count (AFC) numbers of large follicles (≥ 5 mm) in ovaries with US OFD grades I, II and III from group 1.	65
APPENDIX 5 – Graph illustrating the average number of ante-mortem antral follicle count (AFC) in ovaries with US OFD grades I, II and III from group 1.	66
APPENDIX 6 - Graph illustrating the number of ante-mortem antral follicle count (AFC) in ovaries with US OFD grades I, II and III from group 1.	66
APPENDIX 7 - Graph illustrating the average of post-mortem antral follicle count (AFC) numbers of small follicles (<4mm) in ovaries with US OFD grades III and IV from group 1.	67
APPENDIX 8 - Graph illustrating the numbers of post-mortem antral follicle count (AFC) numbers of small follicles (<4mm) in ovaries with US OFD grades III and IV from group 1.	67

APPENDIX 9 - Graph illustrating the average of post-mortem antral follicle count (AFC) numbers of large follicles ($\geq 5\text{mm}$) in ovaries with US OFD grades III and IV from group 1.	68
APPENDIX 10 - Graph illustrating the post-mortem antral follicle count (AFC) numbers of large follicles ($\geq 5\text{mm}$) in ovaries with US OFD grades III and IV from group 1.	68
APPENDIX 11 - Graph illustrating the average number of post-mortem antral follicle count (AFC) in ovaries with US OFD grades III and IV from group 1.	69
APPENDIX 12 - Graph illustrating the number of post-mortem antral follicle count (AFC) in ovaries with US OFD grades III and IV from group 1.	69
APPENDIX 13 – Graph illustrating the average of ante-mortem antral follicle count (AFC) number of small follicles ($< 4\text{mm}$) in ovaries with US OFD grades I, II, III and IV from group 2.	70
APPENDIX 14 - Graph illustrating the ante-mortem antral follicle count (AFC) numbers of small follicles ($< 4\text{mm}$) in ovaries with US OFD grades I, II, III and IV from group 2.	70
APPENDIX 15 - Graph illustrating the average of ante-mortem antral follicle count (AFC) numbers of large follicles ($\geq 5\text{mm}$) in ovaries with US OFD grades I, II, III and IV from group 2.	71
APPENDIX 16 - Graph illustrating the ante-mortem antral follicle count (AFC) numbers of large follicles ($\geq 5\text{mm}$) in ovaries with US OFD grades I, II, III and IV from group 2.	71

APPENDIX 17 - Graph illustrating the average number of ante-mortem antral follicle count (AFC) in ovaries with US OFD grades I, II, III and IV from group 2.	72
APPENDIX 18 - Graph illustrating the number of ante-mortem antral follicle count (AFC) in ovaries with US OFD grades I, II, III and IV from group 2.	72
APPENDIX 19 - Graph illustrating the average of post-mortem antral follicle count (AFC) numbers of small follicles (<4mm) in ovaries with US OFD grades II, III and IV from group 2.	73
APPENDIX 20 - Graph illustrating the numbers of post-mortem antral follicle count (AFC) numbers of small follicles (<4mm) in ovaries with US OFD grades II, III and IV from group 2.	73
APPENDIX 21 - Graph illustrating the average of post-mortem antral follicle count (AFC) numbers of large follicles (≥ 5 mm) in ovaries with US OFD grades II, III and IV from group 2.	74
APPENDIX 22 - Graph illustrating the post-mortem antral follicle count (AFC) numbers of large follicles (≥ 5 mm) in ovaries with US OFD grades II, III and IV from group 2.	74
APPENDIX 23 - Graph illustrating the average number of post-mortem antral follicle count (AFC) in ovaries with US OFD grades II, III and IV from group 2.	75
APPENDIX 24 - Graph illustrating the number of post-mortem antral follicle count (AFC) in ovaries with US OFD grades II, III and IV from group 2.	75

APPENDIX 25 - Graph illustrating the average number of post-mortem antral follicle count (AFC) in ovaries with US OFD grade I from group 3.	76
APPENDIX 26 – Ante-mortem US, Post-mortem US and Histology data for Group 1.	77
APPENDIX 27 - Ante-mortem US, Post-mortem US and Histology data for Group 2.	78
APPENDIX 28 - Ante-mortem US, Post-mortem US and Histology data for Group 3.	79
APPENDIX 29 - Ante-mortem US, Post-mortem US and Histology Comparison for all 3 Groups.	79

ABREVIATIONS

Ovarian follicular dysplasia (OFD)
Granulosa Theca Cell Tumor (GTCT)
Megahertz (MHz)
Ultrasound (US)
Magnetic resonance imaging (MRI)
Computed tomography (CT)
Sex-determining region of Y chromosome (SRY)
Wilm's Tumor factor (WT1)
Steroidogenic factor-1 (SF-1)
Testicular-determining factor (TDF)
Anti-Mullerian hormone (AMH)
Testosterone (T₂)
Dihydrotestosterone (DHT)
Deoxyribonucleic acid (DNA)
Luteinizing hormone (LH)
Follicle stimulating hormone (FSH)
Gonadotrophin-releasing hormone (GnRH)
Corpora haemorrhagica (CH)
Corpora lutea (CL)
Complete mid-sagittal para-hilus histologic section (CMPHS)
Antral follicle count (AFC)
Histological follicular number (HFol)
Ante-mortem ultrasound follicular number (AFol)

I. INTRODUCTION

A study commissioned by Florida Cattleman's Association, which originated in 2007 and continued in 2016, had the goal of finding the major cause of subfertility and infertility in the Florida beef herd. The Florida Cattleman's Association sponsored the study because, by producer's estimates, Florida is below the national average for calf production (cow-calf ratio). In 2007, over 170 beef female reproductive tracts, from eight different ranches, were collected from slaughterhouses and examined. It is important to state that all of these cows were from the culling pens. A significant number of the ovaries from the culled cows contained similar histologic findings. Collectively, these findings were termed ovarian follicular dysplasia (OFD) (Roberts et al 2008; Buergelt et al, 2010). Roberts et al (2008) believed that the term dysplasia, from Küber (2002), was the closest to these ovarian histological findings.

Ovarian follicular dysplasia is a slowly progressive, bilateral abnormal growth and/or development of ovarian follicles (Roberts et al, 2008; Buergelt et al, 2010; Roberts, 2017). This dysplasia is believed to eventually transform the follicles and ovarian stroma into Sertoli-form Granulosa Theca Cells Tumor (GTCT) (Roberts, 2008; Buergelt et al, 2010; Gard et al, 2016). Sertoli-form Granulosa Cell Tumor was first reported by Norris (1969). Ovarian follicular dysplasia has been recognized in recent years by skilled bovine practitioners while performing rectal ultrasonography for evaluation of the reproductive status in beef cows (Gard et al, 2016).

There is no evidence of OFD in veterinary pathology or animal science literature. Reports of bovine ovarian histology linked to subfertility and/or infertility are limited to ovarian tumors or ovarian cystic disease (Roberts, 2017). There is only one study that contains general microscopy describing ovaries from twenty infertile dairy cows in Estonia (Küber & Jalakas, 2002). In this study, researchers documented small cystic degeneration of ovarian follicles, dysplasia of all follicular stages, hyperplasia of cortical stroma and rete ovarii, and suspected preneoplastic changes of the granulosa cells (Küber & Jalakas, 2002). The findings in this study were consistent with what is seen in cattle with OFD (Roberts, 2017).

In 2016, studies showed that later stages of OFD, grades III and IV, could be detected via ultrasound examination of the ovaries when using a 5-7MHz probe (Roberts et al, 2016; Gard et al, 2016). According to these studies, the grades of OFD (III and IV) have decreased numbers of Graafian follicles which can be easily visualized ultrasonographically. Additionally, significant multifocal hyperechogenic areas within the ovary can be visualized (Roberts et al, 2016; Gard et al, 2016).

As the OFD progresses, folliculogenesis, ovulation, and establishment of pregnancy are all negatively affected. This leads to subfertility and ultimately to infertility. The follicular dysplasia also triggers dystrophic mineralization within the ovaries. These mineralized areas can be seen throughout the ovary on histologic analysis (Roberts et al, 2008). The areas of hyperechogenicity seen on ultrasound examination of the ovaries are thought to be areas of calcification, fibrosis, abscessation and/or adipose tissue. These structures have the same ultrasonographic appearance as bone (dense tissues) and therefore cannot be differentiated via rectal ultrasound examination. Ovarian

cysts, small follicular cysts (approximately 0.5 to 1.0 cm) and mucometra can all be visualized via ultrasound and are associated with OFD.

In 2016, thirty *Bos t. indicus* (Brahman) x *Bos t. taurus* (Angus, Simmental, Charolais) beef heifers and cows were examined at two different ranches. According to their local veterinarian, 28 animals were classified as OFD positive via rectal ultrasonography, and two cows were classified as negative control animals. Rectal ultrasound images were collected at both ranches. The following day, these animals were followed to the slaughterhouse for the collection of post-mortem samples.

In addition to this study, a 2017 project utilized five *Bos t. taurus* x *Bos t. taurus* (Angus, Simmental, Charolais) beef cows purchased from North Auburn University Research Unit, located in Auburn, Alabama. Prior to purchase, these five cows were classified as normal multiparous cows. A normal multiparous cow was defined as a cow having at least one calf in the last two breeding seasons (one calf per breeding season) (Gard et al, 2016). These normal multiparous cows were also free of diseases according to the herdsman's history and regular testing. These cows were tested for BVDV via ear notch utilizing an IDEXX ELIZA (IDEXX Laboratories, Westbrook, Maine, USA) and found to be negative. The cows underwent additional testing for BHV-1 via virus isolation on plasma at the Thompson-Bishop-Sparks Alabama State Veterinary Diagnostic Laboratory, Auburn, AL and were found to be negative. The cows were also determined to be negative for *Anaplasma marginale*, *Neospora caninum*, *Brucella abortus*, and *Leptospira spp* through validated tests at the Thompson-Bishop-Sparks Alabama State Veterinary Diagnostic Laboratory.

These cows were submitted for rectal ultrasonographic examination as was done previously in the cows from Florida. All images were recorded and evaluated for degrees of hyperechogenicity and antral follicular count within the ovaries. All ten ovaries were also examined histologically, and the findings were recorded. These five cows were introduced into the study to compare the results and findings from an outside population with those from Florida.

This study is a “branch” of the main research aimed at discovering a practical “chute-side” test for on-farm ante-mortem diagnosis of OFD to minimize producers’ financial losses. The objective of this aspect of the study is to assess the accuracy of ultrasound (US) examination of ovaries in detecting stages of OFD. A 7MHz linear probe was used for ante-mortem analysis of the ovaries. An 8MHz probe was used for post-mortem analysis of the ovaries. The hypothesis was that the 8MHz probe would provide a more defined image allowing for reliable detection of earlier stages of OFD. In addition, thirty ovaries were submitted for magnetic resonance imaging (MRI) and five were submitted for computed tomography (CT). All the data collected from ante-mortem and post-mortem ultrasound examination were blindly compared against OFD grades identified by histology. The images from MRI and CT were briefly analyzed for possible comparison between histological OFD grades.

II. LITERATURE REVIEW

Anatomical structures

The main components of the female reproductive tract include the ovaries, oviducts, uterus, cervix, vagina and external genitalia. In domestic species, the female reproductive tract lies beneath the rectum, with separation by the rectogenital pouch. Because of their size and anatomy, the reproductive tracts of large animals can be examined via rectal manual palpation and ultrasonic examination. This can provide important information regarding ovarian status, pregnancy status, and possible abnormalities within the tract. Also, it can be utilized for advanced techniques such as artificial insemination, embryo transfer, and oocyte collection (Senger, 2012).

The ovary is supported by the cranial part of the broad ligament. This portion of the broad ligament is called the mesovarium. The ovary has a region called the hilus where the ovarian blood and lymphatic vessels and nerves are housed within the mesovarium. Another structure that helps to support the ovaries is the utero-ovarian ligament. This ligament is sometimes referred to as the proper ligament of the ovary (Senger, 2012).

The mesosalpinx is a serous portion of the broad ligament that surrounds and supports the oviduct. Along with supporting the oviducts, the mesosalpinx also envelops the ovary, creating a pocket or bursa. When ovulation occurs, the oocyte is released from the ovarian follicle, and the bursa surrounding the ovary helps to orient the infundibulum, increasing the chances of that oocyte entering the oviduct (Senger, 2012).

In the cow, the size of the ovaries is relatively small compared to the size of the species. After puberty, each bovine ovary is on average about 4 cm long, 2 cm wide, and 2 cm thick. The surface of the ovary surrounding the attachment of the mesovarium is smooth, but the remaining surface is uneven as the result of multiple follicles, corpora lutea and/or corpora albicantia (Schatten & Constantinescu, 2007).

The ovaries, in nulliparous and primiparous cows, are found within the pelvic inlet. The more pregnancies the cow has had, the more cranially the ovaries are located; they drop within the abdominal cavity, pulled by the increasingly larger uterus (Schatten & Constantinescu, 2007).

Embryogenesis

While the conceptus is still a fetus, the development of the reproductive tract takes place in a retroperitoneal position. This means that it is located outside of the peritoneal cavity but is surrounded on one side by peritoneum. As the reproductive tract grows, it begins to push against the peritoneum, becoming suspended within the peritoneal cavity. At this point the tract is surrounded entirely by the peritoneum. A part of this peritoneum eventually forms a double layered sheet of connective tissue. This sheet of connective tissue is called the broad ligament. The broad ligament is responsible for suspending the ovaries, oviducts, uterus, cervix and the cranial vagina within the peritoneal cavity. The broad ligament also houses the vascular supply, the lymphatic drainage and nerves supporting the tract (Senger, 2012).

The combination of chromosomal genotype (XX or XY), gonadogenesis, and the formation and maturation of accessory reproductive glands and genitalia are fundamental

for the formation of a viable and fertile offspring once it has gone through puberty (Gard, 2003).

During embryogenesis, the germ layers cells differentiate into various cells, constituting all parts of the embryo (Senger, 2012). A hypothalamic-pituitary-adrenal-gonadal axis is fundamental for the development of normal sexual differentiation. The genetic components are the foundation for sexual determination of the bipotential gonad. An understanding of the genetic mechanism involved in normal gonadal determination is crucial. The presence of a Y chromosome does not guarantee a male phenotype nor does XX (the absence of Y) guarantees a female phenotype. Genes like SRY (sex-determining region of Y chromosome), combined with non-Y linked genes (WNT-4, WTI, DAX1, SF1 and SOX9) are fundamental for normal gonadal differentiation (Gard, 2003; Naillat, 2015). The normal development of the mammalian urogenital system is among the most complex in the body and critical timing for successful formation is needed (Senger, 2012).

The germ layers are formed from the embryo's inner cell mass during embryogenesis. Prior to uterine attachment the three germ layers that compose an embryo are the endoderm, mesoderm and ectoderm. These layers differentiate, eventually giving rise to all of the tissues, organs and systems present within the normal fetus. The endoderm, the innermost cellular layer of the embryo gives rise to the digestive tract, liver, pancreas, lungs and endocrine organs. The mesoderm gives rise to the circulatory, skeletal, muscular, and urinary system. The reproductive system including gonads, uterus, cervix, cranial vaginal, epididymis, ductus deferens and accessory glands, (depending on the sex of the fetus) mostly originate from the mesoderm. The ectoderm,

or outermost layer, gives rise to the central nervous system, sense organs, mammary glands, sweat glands, skin, hair, claws and hooves (Senger, 2012).

Sexual differentiation

The initial step in sex determination occurs during fertilization when a sperm delivers either an X or Y chromosome to the oocyte (Senger, 2012). The sex of the individual is determined by the sperm, whose chromosome establishes the eventual genetic control of sexual differentiation. Primordial germ cells develop in the early embryo, during the first 15% of gestation, when the yolk sac is still present. These cells originate from the inner lining of the yolk sac and migrate into the hindgut, ultimately inhabiting the undifferentiated gonad. This migration occurs around day 40 of fetal development in cattle. A small number of these cells migrate through the yolk sac mesentery to the developing genital ridge forming the bipotential gonad (Hunt & LeMaire-Adkins, 1997). The genital ridge is located on the inner surface of the dorsal body wall, medial to the embryonic kidneys (mesonephros).

The genital ridge is populated by most of the primordial germ cells bound by epithelium. The primordial germ cells that do not reside in this region will degenerate. The primordial germ cells undergo mitosis during migration to the genital ridge, so their numbers increase significantly. Arrival of the primitive germ cells to the genital ridge triggers the proliferation of connective tissue. The new connective tissue will give rise to compact strands of tissue known as primitive sex cords. The proliferation of these sex cords causes enlargement of the genital ridge toward the developing mesonephros (Senger, 2012).

During embryonic development three distinct renal systems develop. The initial, and most primitive, is termed the pronephros. This non-functional system eventually regresses and is replaced the mesonephros. The mesonephros is a bilateral pair of functional kidneys. The mesonephros produce urine that is drained by a pair of ducts called mesonephric ducts or Wolffian ducts. The final renal system to develop is termed the metanephros. By the first 30% to 35% of gestation, the metanephros are developed and fully functional. These will serve as the kidneys in the adult animal once they develop nephrons (Capel, 1996; Senger, 2012).

During the development of the mesonephros, a second pair of ducts (paramesonephric ducts or Müllerian ducts) also start to develop alongside the mesonephric ducts. Under appropriate conditions, the mesonephric duct gives rise to parts of the male reproductive tract while the paramesonephric ducts give rise to much of the female tubular genitalia. Both ducts are present early in embryonic development in both males and females making it impossible to differentiate them morphologically at this stage (Gard, 2003). This stage of embryogenesis is referred to as the indifferent stage because by simple observation, the phenotypic characterization of sex can not be observed (Capel, 1996; Senger, 2012).

In the normal female, the paramesonephric ducts form the oviducts, uterus, cervix and the cranial vagina. The formation and differentiation of the fetus' appropriate genitalia according to its genetic components, is dependent on the adequate production of appropriate hormones. Some specific genes like Wilm's Tumor factor (WT1) and Steroidogenic factor-1 (SF-1) are associated with normal formation of bipotential gonads (Hattie, 1992; Parker, Shimmer & Schedl, 1999; Gard, 2003).

The undifferentiated gonad consists of primordial germ cells bounded by epithelium. In addition to the germ cells present in males and females, there are three lineages of somatic cells that are found in the adult ovary and testis. One of the lineages develops into support cells, namely follicle cells in females and Sertoli cells in males. A second lineage develops into steroidogenic cells, which are the theca interna cells in females and Leydig cells in males. The third lineage develops into stromal cells in females and myoid cells in males. These cells are responsible for forming the connective tissue, blood vessels and tunica of both organs (Capel, 1996; Gard, 2003).

Differentiation of the gonad into a testis requires presence of testicular-determining factor (TDF), a substance produced by an isolated gene from the SRY, a location present solely on the Y chromosome. In the presence of TDF, cells in the primitive gonad differentiate into Sertoli cells. Sertoli cells are responsible for producing anti-Mullerian hormone (AMH), a hormone that stimulates the Leydig cells to produce testosterone (T₂). In males, testosterone is converted in part to dihydrotestosterone (DHT) by 5 α -reductase. This conversion is needed for the growth, development and secretory activity of the accessory sex organs in the male (Capel, 1996; Gard, 2003). The presence of DHT allows the development of the male phenotype expressed in the adult animal.

Female embryos (XX), lack the gene required for TDF production. In the absence of TDF, the cells in the primitive gonad do not differentiate into Sertoli cells. Hence, the corresponding hormones (testosterone, DHT) cannot be produced. Instead, cells of the sex cords differentiate into primitive follicular cells and the majority of the genital ridge

becomes the ovary. In females, the Müllerian ducts develop in the absence of testosterone and Müllerian Inhibiting Substance, also called AMH (Senger, 2012).

If the TDF is absent, fragmentation of epithelial cords (sex cords) occurs, forming cellular clusters surrounding central primitive germ cells. In females, these clusters of germ cells penetrate less deeply in the interior of the future ovary than in the male. Thus, primordial follicles are formed along the surface of the ovary. This portion of the ovary will eventually become the ovarian cortex. In the ovary, the rete tubule formation is not prominent and the connection between the rete tubules and mesonephric tubules does not occur, therefore, a tubular outlet for the gametes is absent (Senger, 2012).

As previously stated, the female embryo's reproductive tubular structures will develop from the paramesonephric ducts. The cranial part of each paramesonephric duct runs beside the mesonephric duct with its cranial part open to the peritoneal cavity and its caudal end abutting the dorsal wall of the urogenital sinus eventually fusing with it (Capel, 1996; Senger, 2012).

Oogenesis

Oogenesis (the production of oocytes) starts early in fetal life. In cattle, approximately 40 cells differentiate into extraembryonic mesoderm for the establishment of the germ cell lineage. These cells migrate to the genital ridge through the yolk sac mesentery, where X-reactivation happens in XX germ cells and mitotic proliferation takes place. The local production of cytokines (kit-ligand and transforming factor B-1) is thought to be the main stimulus responsible for the survival and migration of the germ cells lineage. The mitosis of these cells occurs between approximately 60 to 90 days of

development in the bovine embryo generating approximately 0.5 million germ cells (Hunt & LeMaire-Adkins, 1997; Gard, 2003). Until recently, it was believed that the oocyte population was defined prior to, or shortly after birth. However, Johnson et al. (2004) demonstrated the existence of germline stem cells in the ovaries of mice that sustained oocyte and follicle production (Beker van Woudenberg, 2004). In mice, this process is followed by meiosis and arrest happening in the pachytene stage of prophase I as originally thought to be in cattle (Britt, 2008). Now, research has shown that this arrestment in cattle occurs in the diplotene stage of prophase I (Landim-Alvarenga1 & Maziero, 2014).

There are several signaling pathways responsible for initiating sex differentiation and eventually meiotic division of germ cells destined to become oocytes. The molecular signals responsible for triggering germ cell differentiation in the young female embryo are still poorly understood. Once reactivation of the X chromosome occurs, mitotic replication ensues until the germ cells lose their potential for mitosis (Hunt & LeMaire-Adkins, 1997). The stimulus for these events is thought to originate from the developing ovary. As long as germ cells are not exposed to inhibitory signals from developing testis during the prenatal period, it appears that the meiotic commitment of the cells is independent of external signals. Entry of germ cells into meiosis prophase I indicates a commitment to the female pathway (Hunt & LeMaire-Adkins, 1997; Gard, 2003).

Meiosis is essential for sexual reproduction in most animals and is unique to germ cells (Beker van Woudenburg, 2004). Meiosis is made up of two cycles. During the first cycle, germ cells' chromosomes will duplicate and then recombine into new

chromosomal pairs (crossover). During the second cycle, chromosomes divide without replication resulting in germ cells with only a single strand of deoxyribonucleic acid (DNA) per chromosome. These resultant cells are now called gametes. Cells with only a single strand of DNA are referred to as haploid cells. Recombination in meiosis I results in cells with different DNA sequences on analogous chromosomes (Whitaker, 1996).

In most species, there are two major arrests that occur during meiosis. Bovine oogonia progress through the leptotene and zygotene stages of meiosis I until they enter the diplotene stage, where they reach their first long period of arrest (Britt, 2008). At puberty, follicle growth occurs and meiotic division resumes after luteinizing hormone (LH) stimulates germinal vesicle breakdown (Whitaker, 1996; Gard, 2003). The second arrest occurs at metaphase II right before ovulation. This meiotic division will not resume until the oocyte is exposed to an activated sperm (Beker van Woudenburg, 2004).

Folliculogenesis begins when oocytes enter into meiosis I. The arrested diplotene oocytes become surrounded by a single layer of flattened germinal epithelial cells, later termed granulosa cells. This structure is known as a primordial follicle and is the first stage in folliculogenesis. As folliculogenesis progresses, the oocyte grows, and the granulosa cells begin to enlarge, becoming cuboidal in appearance. This structure is termed the primary follicle. At birth, females have their lifetime's supply of primary follicles (Senger, 2012). The granulosa cells replicate, eventually forming multiple layers around the oocyte, forming the secondary (pre-antral) follicle. The oocyte within the secondary follicle secretes glycoproteins that form the zona pellucida which surrounds the oocyte. This layer of glycoproteins is very important for sperm binding (Hafez & Hafez, 2000; Gard, 2003). Secondary follicles also become surrounded by a layer of

fibroblast-like cells called theca cells at this stage. Antral (tertiary) follicles (also known as Graafian follicles), are the final pre-ovulatory stage of folliculogenesis (Britt, 2008). Antral follicles consist of the oocyte and fluid filled space called the antrum surrounded by multiple layers of granulosa cells. Bordering the granulosa cells is the theca interna layer and outside of that is the theca externa. The theca interna cells produce the androgens in response to LH. Follicle stages prior to the antral stage can only be visualized microscopically. Antral follicles are visible to the naked eye and range from less than 1 mm to multiple centimeters in size, depending on species (Senger, 2012).

It takes approximately 80 to 100 days for folliculogenesis to occur in bovine species. Follicle growth is regulated by signals between the oocyte and the granulosa cells, granulosa cells and other cells in the ovarian cortex, and from signals originating from systemic circulation (Britt, 2008). The granulosa cells themselves secrete a variety of hormones and substances and contain follicle stimulating hormone (FSH) receptors (Shahrokhi, 2018; Senger, 2012). The most notable hormones excreted are estrogen, and inhibin within the follicular fluid. Maturation of the oocytes is believed to be largely dependent on the granulosa cells and their products (Shahrokhi, 2018; Senger, 2012).

Once follicles reach the secondary stage of development, they become responsive to gonadotropins. As concentrations of gonadotropins fluctuate and change, so do follicular waves. There are three major phases that these waves of follicles (antral follicles) undergo: recruitment, selection, and dominance. Cattle typically have two to three follicular waves during each estrous cycle (Senger, 2012).

The follicular phase begins with luteolysis, or lysis of the progesterone producing corpus luteum which results in markedly decreased circulating progesterone

concentrations. The hypothalamus is then stimulated to produce and release gonadotrophin-releasing hormone (GnRH) as the negative feedback from progesterone is removed. It is important to mention that the hypothalamus contains two separate clusters of nerves responsible for secreting GnRH. One is the tonic center and is responsible for basal secretion of GnRH. The other is the surge center and is responsible for the preovulatory release of LH (Senger, 2012). Gonadotrophin releasing hormone stimulates the anterior pituitary to produce FSH and LH.

A wave of antral follicles is recruited into the growing pool by the increase in circulating FSH. In monotocous species like the cow a single (sometimes multiple) follicle grows larger than the rest and becomes the dominant follicle, while in polytocous species there can be several follicles. The remaining smaller follicles will eventually undergo atresia (degeneration). The dominant follicle synthesizes and secretes estradiol as well as inhibin. Inhibin inhibits the release of FSH from the anterior pituitary, stopping the recruitment and growth of other follicles. Appropriate endocrine signals are essential for continual development of follicles and as such, the majority of antral follicles recruited will undergo atresia (Shahrokhi, 2018; Senger, 2012).

The surge of GnRH prior to ovulation is controlled by high concentrations of estrogen and low concentrations of progesterone. Once estrogen reaches a threshold concentration, the surge (preovulatory) center of the hypothalamus is stimulated and large quantities of GnRH are released, stimulating the anterior pituitary to secrete a preovulatory surge of LH (Senger, 2012).

Developing follicles have LH receptors on the cells of the theca interna. Binding of LH to these specific receptors ultimately leads to the conversion of cholesterol to

testosterone, which diffuses out of the thecal cells and into the granulosa cells. The granulosa cells contain FSH receptors, which, when bound by FSH convert the testosterone to estradiol, the hormone responsible for inducing the LH surge. This pathway is often referred to as the 2-cell, 2-gonadotropin pathway and is crucial for development of follicles to the preovulatory stage (Senger, 2012). Binding of the FSH and LH on the granulosa cells is critical for resumption of meiosis to metaphase II and eventually the ovulation of the antral or Graafian follicle (Gard, 2003).

The LH surge initiates degradation of the gap junctions between granulosa cells, resulting in dissociation of the cells (Anderson, 1999; Gard, 2003). The disruption of communication between the oocyte and the granulosa cells is thought to be partially responsible for removing the inhibition of meiosis. It also stimulates the theca interna cells to start producing progesterone instead of testosterone. This progesterone production causes the theca cells to begin synthesizing collagenase, an enzyme that breaks down collagen in connective tissue. The outside of the ovary is covered by a layer of connective tissue called the tunica albuginea, which when exposed to this collagenase begins to break down and weaken in the location where the dominant, preovulatory follicle resides. The apex of the follicle (stigma) thins and the surface of the epithelium degenerates. Prostaglandin released locally from the ovary stimulates ovarian contractions, forcing the stigma to protrude further from the surface of the ovary, eventually resulting in follicular rupture and extrusion of the oocyte (Senger, 2012).

Following ovulation, the remaining granulosa cells and theca interna of the follicle undergo significant transformation into luteal tissue. This process is called

luteinization. Once functional, this luteal tissue is responsible for producing progesterone (Senger, 2012).

Apoptosis

Cells that are damaged, affected by disease, or destined for destruction during embryo development undergo a programmed cell death known as apoptosis. Elimination of specific cells requires very specific genetic and molecular signals that activate coordinated signal transduction events. With the development of transmission electron microscopy, visualization of apoptotic cells has allowed the determination of morphological characteristics associated with apoptosis. The most notable changes are condensation and degradation of chromatin, destruction of cytoskeleton, clustering of nuclear pores, and sequestration of chromatin into membrane-bound apoptotic bodies. These bodies will then be phagocytized by macrophages. The difference between apoptosis and necrosis (non-programmed cell death) is that there is no accompanying inflammation with apoptosis (Schatten & Constantinescu, 2007).

Paraovarian and Ovarian Cysts

There are approximately 16 different types of cysts that can occur within the ovary or its surroundings. Cysts derived from the tubular remnants of mesonephric duct and paramesonephric ducts are included in this group but are considered to be of congenital origin. It is important to know the normal size of mature follicles in diagnosing cystic conditions. Also, a histologic examination of the wall and cells of the cystic structure is necessary for appropriate classification (Schatten & Constantinescu,

2007). Schatten & Constantinescu (2007) state that there are controversies in the literature relative to the histological structures of the cyst wall.

Cystic structures that arise in females from remnants of the mesonephric tubules and are called paraovarian cysts. The cysts that result from the cranial mesonephric tubules are classified as cysts of the epoophoron. A variation in size from millimeters to centimeters in diameter can be seen in these cysts. They are filled with clear fluid and can be present in neonates. Bursal cysts develop when there are adhesions of the fimbria to the ovary. Bursal cysts contain fluid from the uterine tube that flows into the bursa. In the presence of salpingitis, accumulation of clear fluid may be seen refluxing from parts of the uterine tube into the bursa (Schatten & Constantinescu, 2007).

The most frequently recognized form of intraovarian cystic degeneration is a Graafian (follicular) cyst. The condition starts when the animal is in estrus. One proposed pathophysiologic mechanism of follicular cyst formation is the failure of estrogen production and stimulation of LH release. When a mature antral follicle is not stimulated to ovulate, it increases in size due to fluid accumulation. Signs of anestrus, irregular estrus, or nymphomania can be observed in the animals with follicular cysts. Also, the affected animals can have uterine hydrometra or mucometra due to a chronic ovarian cystic condition (Schatten & Constantinescu, 2007).

An anovulatory, luteinized, follicular cyst is defined as a mature, dominant, antral follicle that failed to ovulate but underwent luteinization. An ovulatory papilla is absent from the surface of the ovary. The spherical cyst contains a large amount of fluid within its cavity and the luteinized wall is uniform in thickness (Schatten & Constantinescu, 2007).

Cystic corpora lutea (also known as cystic CLs) are defined by the occurrence of ovulation, but with a persistent fluid center within the CL's interior. The ovulation papilla is present in this case. The wall thickness and outline of the cystic CL may be irregular. There is no clinical significance, as they function like a normal CL and can be present in pregnant cows. There is a large variation in size of the fluid-filled spaces, and they are extremely common (Schatten & Constantinescu, 2007).

Buergelt (1997) stated that "cystic endometrial hyperplasia may develop endogenously, secondary to follicular ovarian cysts or granulosa cell tumors." In ruminants, pastures with estrogen-containing plants (clover and alfalfa) may act as exogenous sources, resulting in cystic endometrial hyperplasia (Buergelt, 1997).

Granulosa-Theca Cell and Sertoli Cell Tumors

Baba & Cătoi (2007) stated that "sex cord-stromal tumors are formed from gonadal, medullary or cortical stroma, and from granulosa cells and theca interna cells." These tumors have the capability to produce and release active steroid hormones (estrogen and/or progesterone). These neoplasms are named and classified depending on the predominant type of cells and their origin (Baba & Cătoi, 2007).

These sex cord-stromal tumors are more commonly diagnosed in cows and mares when compared with other species. Old cows and cows under 4 years of age have a higher incidence. Animals with these tumors can present with unchanged behavior or they can present with signs of an oversecretion of estrogens and androgens (nymphomania). The estrous cycle of the affected animals is usually irregular, prolonged or absent (infertile) (Baba & Cătoi, 2007).

In cows and mares, these tumors are, in most cases unilateral and 10 to 23 centimeters in diameter. They are found in a spherical or ovoid shape, lobulated, with a sparse to dense consistency. Also, they are usually encapsulated within the ovary and the color is yellow-gray, with red bands and cysts that have a watery, red-brown or yellow content. Hemorrhagic and/or necrotic foci commonly appear in section (Baba & Cătoi, 2007).

Granulosa-Theca cell tumors (GTCT) or granulosa cell tumors are benign and unilateral, and increased incidence with age, but can also be present in young animals. Microscopically, the GTCT cells are like normal granulosa cells. The cells appear as a uniform population, with poorly colored cytoplasm, and are poorly delineated, with round or ovoid eccentric nuclei, and few or no mitotic figures (Baba & Cătoi, 2007).

Neoplastic cells can be arranged as a diffuse sarcoma with long cords, islands delineated by connective septa and follicles with Call-Exner bodies which is similar to what is seen in granulosa cells in humans. Baba & Cătoi (2007) also stated that “some cells have abundant, poorly colored cytoplasm, similar to testicular Sertoli cells; the connective stroma being well represented in the tumor mass. Tumors formed by granulosa cells and Sertoli cell tumors have been described in cows but with a smaller incidence than in mares (Baba & Cătoi, 2007).

The microfollicular structure of granulosa cells neoplasia consists of follicles of variable sizes and are lined by cells similar to follicular epithelium with normal-sized antral follicle. The cells are arranged in one or multiple layers. The lumina of microfollicles contain a granular or acidophilic, homogenous material. Neoplastic cells in the form of solid masses or small rosettes have been reported in the literature, suggesting

embryonic follicles. These cells are round, ovoid, or fusiform, similar to normal follicular cells. There is a large variation in sizes with ovoid or round, hyperchromatic nuclei and the presence of a vacuoles in the cytoplasm. Mitotic figures are observed, sometimes in high numbers (Baba & Câtoi, 2007).

The neoplasms formed by Sertoli cells show microscopically a tubular or fascicular growth, with connective septa. These cells have a vacuolated cytoplasm, and amphophilic staining. Also, these cells have an elongated shape and sharp tips with fusiform cells being atypical. The nuclei are small, uniform, and vesicular. The nucleoli are inapparent and mitotic figures are rare. In animals, Sertoli cell tumors are not identical to those seen in women. In women, Leydig cells with immature mesenchymal structure also appear. The common origin (of the primordial tissues) of female and male gonads may help to explain the presence of Sertoli cells in the ovary (Baba & Câtoi, 2007).

Ultrasonography

Ultrasonographic examination of animals has become a common practice among veterinarians. In the past, when ultrasound machines were brought to the field of veterinary medicine, most were used for research purposes only. The two most important reasons were first, the high costs and second, the size of the equipment itself, combined with the need for an external power source. With the evolution of ultrasound technology, many machines are now portable, with easy setup (internal power sources), and lower prices have made these machines more accessible to private operations and businesses.

In 1995, O. J. Ginther stated that gray-scale diagnostic ultrasonography is the most profound technological advance in the field of large animal research and clinical reproduction since the introduction of transrectal palpation and radioimmunoassay of circulating hormones. In retrospect, the volume of research and commercial application of this technology over the last three decades support his statement.

Ultrasound examination of the bovine reproductive tract has been utilized more frequently and is part of daily reproductive procedures performed by many bovine practitioners around the world. The bovine reproductive tract is most commonly scanned via the rectum with a real-time, B-mode, transrectal linear-array probe, also known as transrectal transducer. Linear-array transducers are composed of a series of piezo electric crystals arranged in a row. When energized, these crystals emit, and alternately receive, high frequency sound waves. This configuration (linear-array) results in a rectangular image of the field of scan (Fricke & Lamb, 2002).

Ovarian activity has been reviewed with ultrasonographic examination in great detail. The ovarian structures that can be identified with real-time ultrasound are ovarian stroma, ovarian vessels, antral follicles, cysts, corpora haemorrhagica (CH) and corpora lutea (CL) (Pierson & Ginther, 1988). Because antral follicles are fluid filled structures, they are the most recognizable structure within an ovary. The fluid filled cavity is easily seen in the ultrasound image as black (anechoic or non-echogenic). Structures like ovarian stroma, CH and CL contain different degrees of dense cells, which result in different echogenic densities of gray/white on the ultrasound screen. Therefore, ultrasound examination of ovaries is a highly accurate and a rapid method to assess where the animal is in correlation with its estrous cycle. Unfortunately, during pregnancy

diagnosis, bovine practitioners tend to proceed directly to the uterus and neglect the ovaries. Knowing that the ovaries contain a wealth of information about the animal's reproductive status, this habit can interfere negatively when appropriate therapies or reproductive interventions are needed (Fricke & Lamb, 2002).

III. JOURNAL ARTICLE

STATEMENT OF RESEARCH OBJECTIVES

The hypothesis of this study was that the 8MHz linear probe would provide a more defined image allowing for detection of earlier stages of OFD. For ante-mortem evaluation, a 7MHz linear probe was used versus an 8MHz probe for post-mortem evaluation. Some ovaries were submitted for magnetic resonance imaging (MRI) and computed tomography (CT) for further analysis. All the data sets collected from ante-mortem and post-mortem ultrasound examination, MRI, and histology were blindly compared against OFD grades in 35 individual beef cows. The objective of this study was to assess the accuracy of ultrasound examination of ovaries in detecting stages of OFD.

MATERIALS AND METHODS

Animals

In 2016, two groups of 15 *Bos t. indicus* (Brahman) x *Bos t. taurus* (Angus, Simmental, Charolais) females from two different ranches located in the state of Florida were included in the OFD study. All of these animals had different breed compositions, but all had Brahman influence. The first group (group 1) was composed of 15 heifers, and the second group (group 2) was comprised of 15 cows. The cows included in group 2 were a mixture of primiparous and multiparous cows. The cattle from groups 1 and 2 were selected randomly from the culling pens of their respective ranches. Twenty-eight of these animals (14 from each group) were called either “open” (not pregnant) by their

local veterinarian for that breeding season and/or the previous breeding season or were non-productive due to a secondary condition that would not allow the female to deliver a viable calf such as; pyometra, mucometra, dead fetus, or an immature reproductive tract. Two animals, one from each group, were normal, cyclic, fertile females according to their local veterinarian. The normal animal from group 1 was a heifer, and the normal animal from group 2 was a multiparous cow. Both normal animals were diagnosed via rectal ultrasound exam to be in the earlier stages of, what seemed to be at the time, a viable pregnancy (first trimester).

In 2017, a third group (group 3) from Auburn, Alabama was introduced into this study. Group 3 had five *Bos t. taurus x Bos t. taurus* (Angus, Simmental, Charolais) brood cows. The five cows were classified normal, multiparous cows (having had 1 calf each, in the two previous breeding seasons).

Prior to the inclusion of the animals in the study, all groups (1, 2 and 3) were tested and found to be negative for the following infectious diseases: *Tritrichomonas foetus*, *Campylobacter fetus* subspecies *venerealis*, Bovine Viral Diarrhea virus, Bovine Herpes Virus-1, *Neospora caninum*, and *Leptospira* spp. All animals had a body condition score (BCS) between 4 and 6 on a scale from 1 to 9 (beef cattle body condition score). They were also clinically healthy by visual examination (no lameness, no injuries, no abnormal discharges).

Collection of Ultrasound Images

The ovaries of the 35 animals were evaluated ultrasonographically using two different probes, a 7MHz Ibex PRO and an 8MHz Ibex EVO (E.I. Medical, Loveland,

CO). Rectal linear probes were used for ante-mortem and post-mortem US examination. The machine used for ante-mortem diagnosis was an Ibex PRO. The machine used for acquisition of post-mortem ovarian images (photos and/or videos) was an Ibex EVO. All images were saved for later analysis.

The ante-mortem ultrasound examinations were performed at the ranches (on site) for every heifer and cow. Conventional cattle chutes were used to restrain the animals while multiple samples and images were collected, including rectal ultrasonographic evaluation of the reproductive tracts (ovaries, uteri and cervixes). During the collection of ante-mortem ovarian ultrasound images, the animals were not sedated nor did they receive any local anesthetic block (epidural).

For post-mortem evaluations (ultrasound imaging, gross evaluation and histology), the same ovaries were harvested at the slaughter facility and placed on ice immediately. These ovaries were taken to a separate facility about 2.5 hours away where tissue fixation in 10% buffered neutral formalin (Fisher Scientific, Hampton, NH) was performed. For each ovary, measurements were taken individually, and a complete mid-sagittal para-hilus histologic section (CMPHS) was prepared as previously described.



Figure 1. Reproductive tract samples collected for analysis and placed in labelled containers.

All post-mortem ultrasonographic examinations were performed with each ovary separated and bagged individually. Each plastic pouch (containing one ovary) was submerged in water for better analysis of ovarian structures with the ultrasound machine (Ibex EVO with an 8MHz rectal linear probe). Videos and photos of post-mortem ultrasonography were saved for analysis.

For imaging analysis, the animals had one image from each ovary (right and left) recorded during the ante-mortem ultrasound sampling. These images were graded for areas of hyperechogenicity, number of antral follicles (Appendices 1 to 6 and 13 to 18) and presence or absence of CL and cystic structures. Every animal was evaluated for pregnancy, and all pregnancies were confirmed to be viable with visualization of a fetal heartbeat. If the fetus did not have a heartbeat, then the pregnancy was considered non-viable. For post-mortem examination, a set of 3 to 5 short videos from different angles of the entire ovary were graded individually for areas of hyperechogenicity, number of

antral follicles (Appendices 7 to 12, and 19 to 25) and presence or absence of CL and cystic structures.

The ultrasonographic hyperechogenicity (HEch) score system used for evaluation of the ovaries was based on number of hyperechogenic areas within each ovary. Ovaries that did not have abnormal hyperechogenic areas on ultrasound examination were scored as 0. The ovaries that contained one or multiple hyperechogenic areas on ultrasound were scored on a scale from 1 to 10 based of the number of hyperechoic areas (Table 1). According to the US HEch score, each ovary received an US OFD grade from I to IV as is showed on Table 2.

Ultrasonographic Hyperechogenicity (HEch) Score

HEch Score	# of HEch areas	HEch Score	# of HEch areas
1	1 to 10	6	51 to 60
2	11 to 20	7	61 to 70
3	21 to 30	8	71 to 80
4	31 to 40	9	81 to 90
5	41 to 50	10	≥ 91

Table 1. Ultrasonographic hyperechogenicity scoring system used in evaluation of the ultrasound images.

Ultrasonographic OFD Grade

Grade	US HEch Score
I	1 and 2
II	3 and 4
III	5 and 6
IV	≥ 7

Table 2. Ultrasonographic OFD grading system applied to the ultrasound images.



Figure 2. Fixed ovaries being assembled into plastic pouches for post-mortem ultrasonographic examination.



Figure 3. Image of examination of post-mortem ovaries using the ultrasound machine Ibex EVO.

Later, in the study, 30 ovaries (10 from group 1, 15 from group 2, and 5 from group 3) were submitted for MRI, and five ovaries from group 3 were submitted for CT. The MRI was done as a control and as a comparison with results of ovarian ultrasound. The CT was done to more accurately interpret the hyperechoic areas found on ultrasound and MRI.

Collection of Magnetic Resonance Imaging and Computed Tomography

The thirty ovaries were individually sealed in plastic pouches with minimal air bubbles. Groups of five ovaries were arranged in a plastic box for simultaneous 3D MRI. The plastic box was filled with tap water to fill the air gaps between the ovary pouches. The plastic box of five ovaries was placed in the center of the MRI knee coil for imaging.

The MRI scanner utilized in this study was a 7 Tesla human-size Siemens Magnetom (Siemens, Malvern, PA) with software VB17A (Siemens, Malvern, PA). The MRI coil used was a QED 1-Transmit/28-Receive channel human knee coil. The scan type was a T1-weighted, fast low angle shot (FLASH), true 3D with an in-plane Field of View (FOV) equal to 128 x 96 mm x 57.6 mm. The number of partitions was 144, and the partition thickness was 0.4 mm. The matrix size was 320 x 240 with a pixel/voxel size of 0.4 x 0.4 x 0.4 mm (isometric). The Time of Repetition was 827 ms, and the Time of Echo was 2.35 ms. The flip angle was 10 degrees (non-selective excitation) with a readout bandwidth of 651 Hz/pixel. The average per rack was 6, and the Time of Acquisition was 19 min + 55 sec (per rack).

Five ovaries were also submitted for scanning via 164-slice dual-energy SOMATOM Definition CT unit (Siemens, Malvern, Pa) following MRI. The CT parameters utilized in the scans were a GE Lightspeed VCT 64 Slice CT scanner with a partition thickness of 0.625mm slices. The voltage was 120kV and 800mA. Images were acquired using a detailed reconstruction algorithm for soft tissue. Analysis of the MRIs and CTs of the ovaries were performed utilizing Mimics® software version 14 (Materialise HQ, Leuven, Belgium) and D Studio Max software (Discreet Logic, Montreal, QC, Canada).



Figure 4. Fixed ovaries in plastic pouches grouped together for MRI examination.

Histological Analysis

All ovaries were placed in 10% buffered neutral formalin (Fisher Scientific, Hampton, NH) for tissue fixation. As stated previously, each ovary was measured and a complete mid-sagittal para-hilus histologic section (CMPHS) was prepared. Fixed tissues were embedded in paraffin, cut in 4µm sections with a microtome, mounted on slides, and stained with hematoxylin and eosin (H&E). The H&E staining was performed with a Leica Autostainer XL. Heat was applied for 10 minutes. Hemo-De was applied for eight minutes followed by two more applications at five-minute increments. One hundred per

cent (100%) ethanol was applied twice at two-minute increments followed by 95% ethanol twice at two-minute increments. A wash was then performed. Hematoxylin was applied for five minutes followed by a second wash. Scott's solution was then applied for two minutes. Then, 80% ethanol was applied for two minutes. Eosin stain was applied for 30 seconds. Ethanol was applied at 95% concentration twice at two-minute increments, followed by 100% twice for two minutes. Xylene was then applied three times at two-minute increments.

An anatomic pathologist (JR) evaluated the slides utilizing sub-gross examination and/or a light microscope (Olympus, Shinjuku, Tokyo, Japan). The slides were graded on an OFD grading scale of I to IV, with normal being zero (0). Non-OFD ovaries did not contain individual dysplastic follicles. Ovaries with the granulosa-type GTCT were not included as Grade IV OFD. The slides were graded in accordance with the protocols outlined below:

Grade I OFD contained scattered individual follicles with multiple Call-Exner bodies adjacent to the medulla and formation of Sertoli-form anovulatory cords near the rete ovarii and hilar region.

Grade II OFD had clustered follicles with multiple-Call-Exner bodies that were located in the medulla but also had low numbers ($< 10/\text{CMPHS}$ of cortex) in the cortex.

Grade III OFD had moderate to large numbers of clustered and individual follicles with multiple Call-Exner bodies in the medulla and cortex ($>10/\text{CMPHS}$ of cortex).

Grade IV OFD had variable clusters of follicles with multiple-Call-Exner bodies ($> 1/\text{CMPHS}$) and foci of Sertoli-type GTCT in the medulla or cortex.

In reference to operational efficiency:

Determination of Grade I OFD requires the slide to be examined utilizing a light microscope (Olympus, Shinjuku, Tokyo, Japan) and the mid-range objective (20X). The slide will require examination of approximately 1-2 minutes to detect subtle signs of Grade I OFD (Figure 5) or determine that the ovary is indeed normal (Figure 6).

Determination of Grade II OFD requires the slide to be examined utilizing a light microscope (Olympus, Shinjuku, Tokyo, Japan) and the low power microscope objective (4X). It takes about 20-30 seconds to identify the signs of OFD such as malformation of the secondary follicles (Figure 7).

Determination of Grade III OFD requires the slide to be examined utilizing sub-gross examination of the slide for 2-3 seconds and additional light microscope (Olympus, Shinjuku, Tokyo, Japan) examination with the low power objective (4X) may needed to determine if there is any question if it is a Grade III or a Grade IV OFD (Figure 8).

Determination of Grade IV OFD requires the slide to be examined utilizing sub-gross examination of slides for 2-3 seconds. The severity of OFD is clear with few or no Graafian follicles and severe dystrophic mineralization (Figure 9).

Each ovary was assigned a grade for the amount of dystrophic mineralization present.

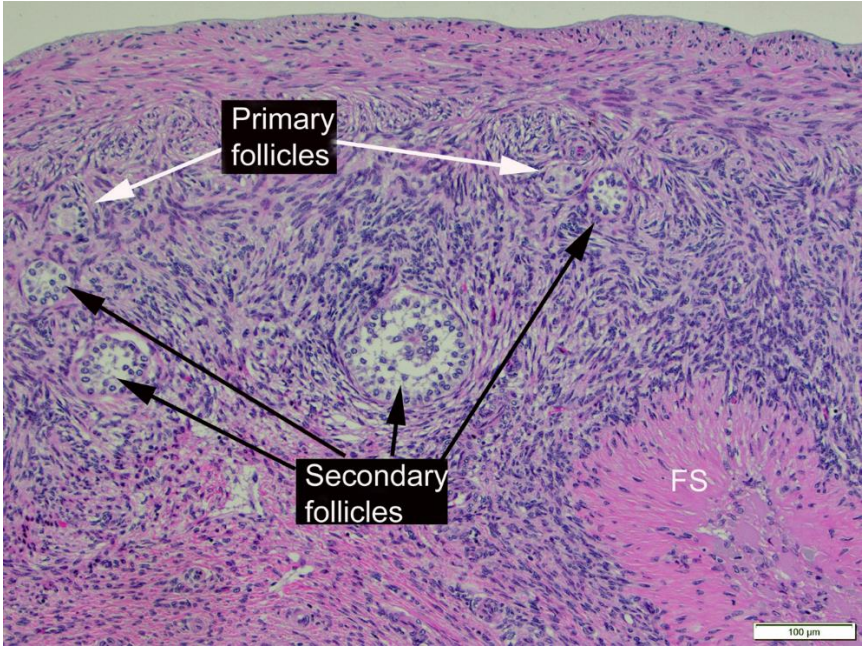


Figure 5. Hematoxylin and eosin stained histologic section of an ovary with Grade I ovarian follicular dysplasia.

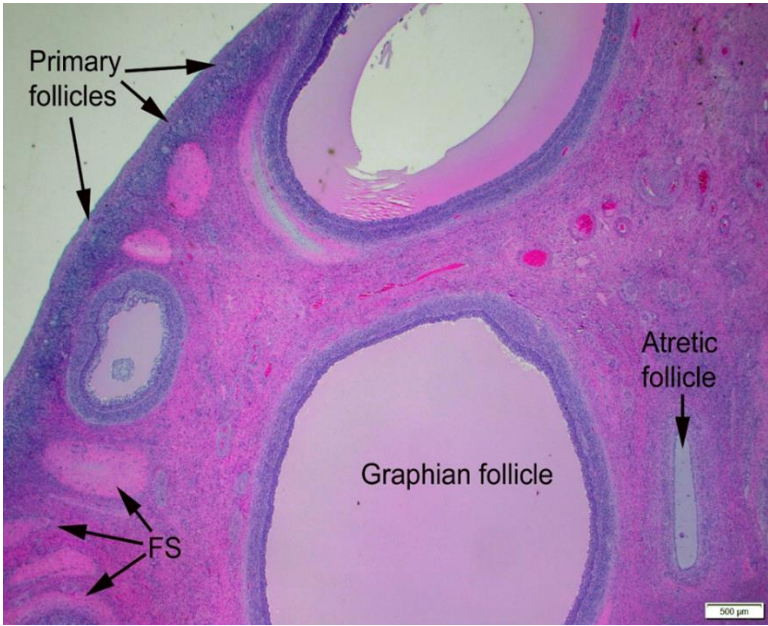


Figure 6. Hematoxylin and eosin stained histologic section of a normal ovary with primary, Graafian, and atritic follicles present within the ovarian stroma.

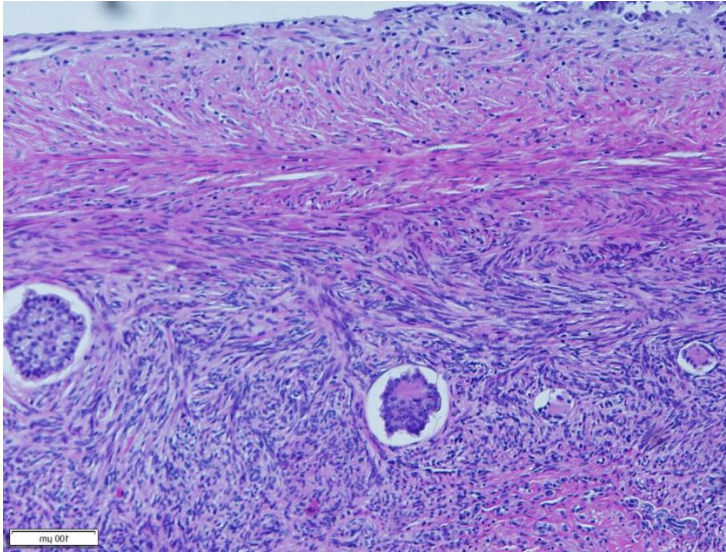


Figure 7. Hematoxylin and eosin stained histologic section of an ovary with grade II ovarian follicular dysplasia. The outer cortex contains equal numbers of primary and secondary follicles.

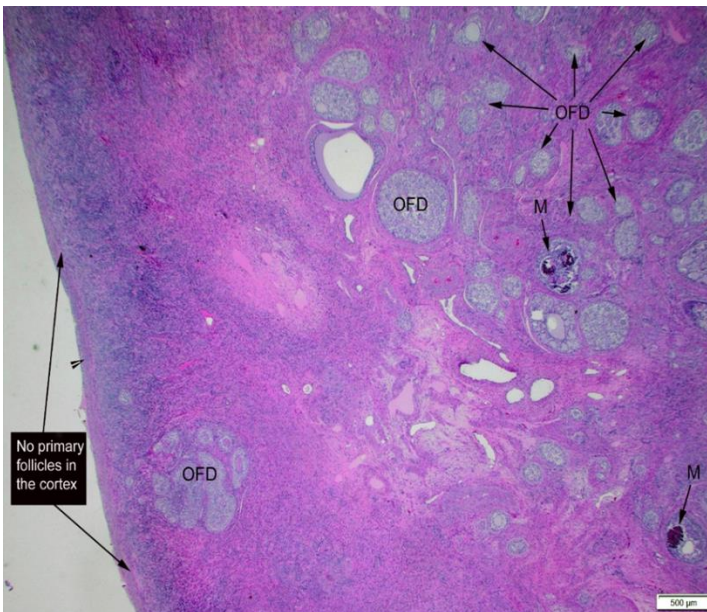


Figure 8. Hematoxylin and eosin stained histologic section of an ovary with grade III ovarian follicular dysplasia.

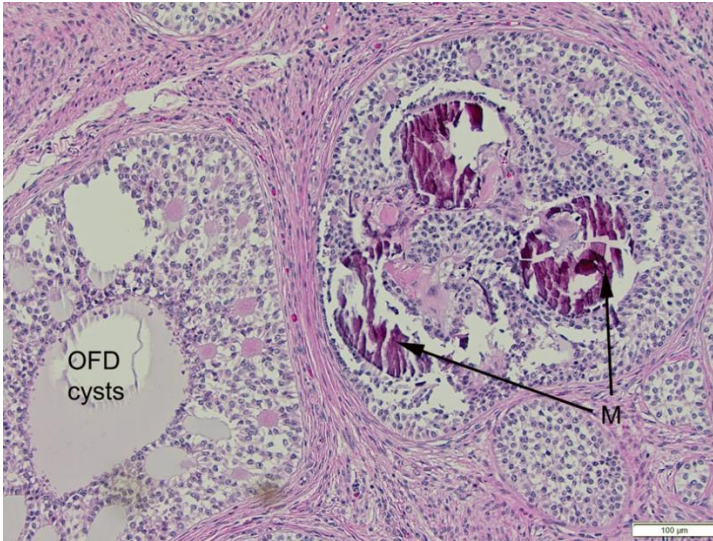


Figure 9. Hematoxylin and eosin stained histologic section of an ovary with grade III ovarian follicular dysplasia (OFD) with central dystrophic mineralization (black arrows labelled M) and developing cysts within dysplastic follicle.

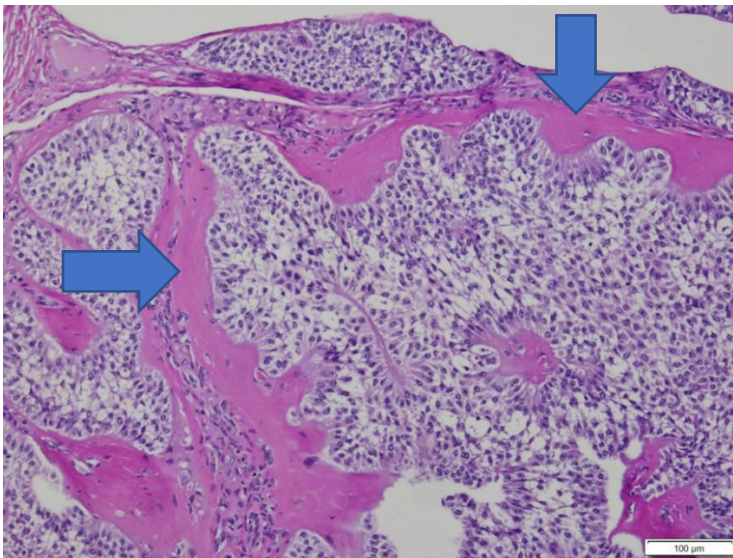


Figure 10. Hematoxylin and eosin stained histologic section of an ovary with grade IV ovarian follicular dysplasia. This benign tumor contains formation of metaplastic bone (arrows).

Statistical Analysis

For the statistical analysis, hypothesis testing was conducted for Pearson correlation analysis. The Pearson correlation coefficient a measure of the linear correlation between two variables X and Y and depicts the extent that a change in one variable affects another variable. The null and alternative hypothesis were as follows: Null hypothesis: the correlation coefficient between two variables = 0 and the Alternative hypothesis: correlation coefficient between two variables $\neq 0$. The significant level or α , was considered to be $p < 0.05$. The R software (<https://www.r-project.org/about.html>) (Free Software Foundation, Boston, MA) was used for this analysis.

RESULTS

The only method for definitive diagnosis of OFD has been via histologic examination of the ovaries. However, OFD has now begun to be characterized in more detail clinically (Roberts, 2008; Buergelt, 2010; Roberts, 2016; Roberts, 2017 unpublished), and clinical evidence of this abnormal condition is able to be detected via additional modalities such as ultrasound examination (Gard, 2016).

According to histologic examination of the ovaries, the combination of sample groups 1 and 2 had a total of 24 of 28 animals positive for OFD. This represents 85.7% of the animals from the culling pens from Florida. The other two animals (normal controls, 1 heifer in group 1 and 1 cow in group 2) from Florida were confirmed to be negative for OFD via histology. Ten animals from group 1 were positive for presence of OFD. Of these ten heifers, all had grade I OFD (66.6%) upon histological analysis. A total of 14 animals from group 2 were positive for OFD (93.3%) with seven as grade I OFD

(46.6%), five as grade II OFD (33.3%) and two as grade III OFD (13.3%) upon histologic analysis. No ovary with grade IV OFD by histologic evaluation was seen in this study.

The multiple areas of hyperechogenicity indicative of mineralization, adipose tissue, abscessation and/or fibrosis, and the presence of cystic areas within the ovaries were detected via trans-rectal ultrasound of the OFD positive cattle (Figures 11-18).

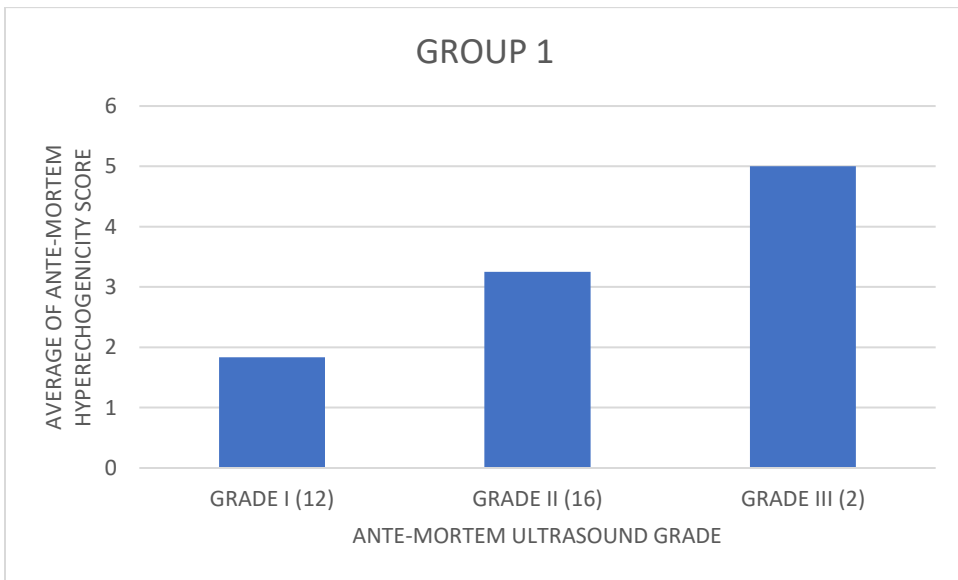


Figure 11. Graph illustrating the ante-mortem average scores of US hyperechogenicity and US OFD grades of ovaries in group 1.

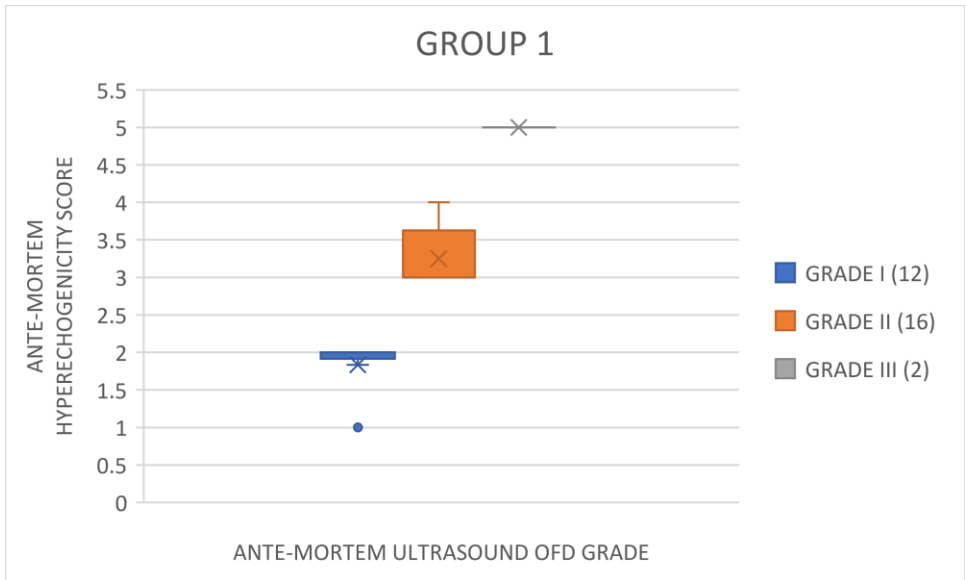


Figure 12. Graph illustrating the ante-mortem US hyperechogenicity scores and US OFD grades of ovaries in group 1.

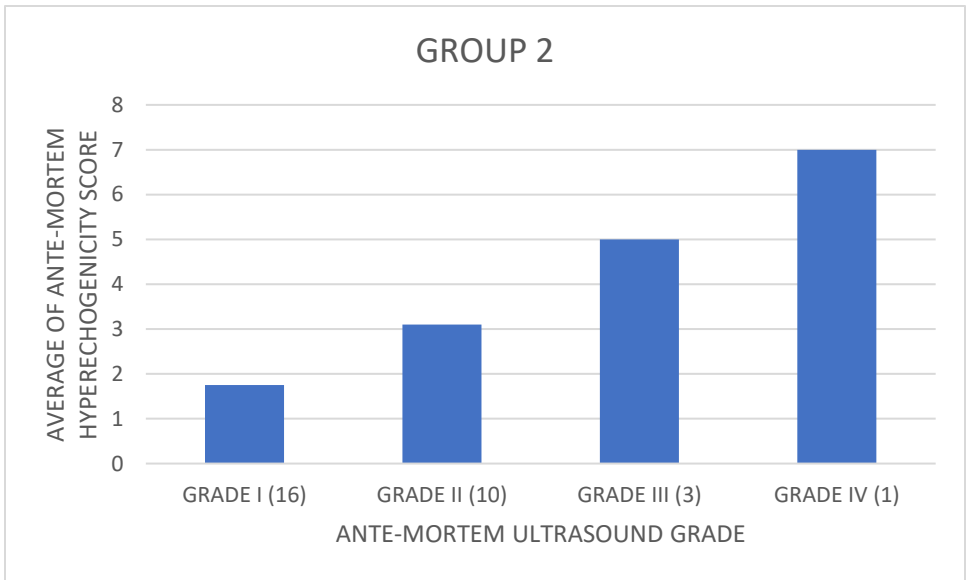


Figure 13. Graph illustrating the ante-mortem average scores of US hyperechogenicity and US OFD grades of ovaries in group 2.

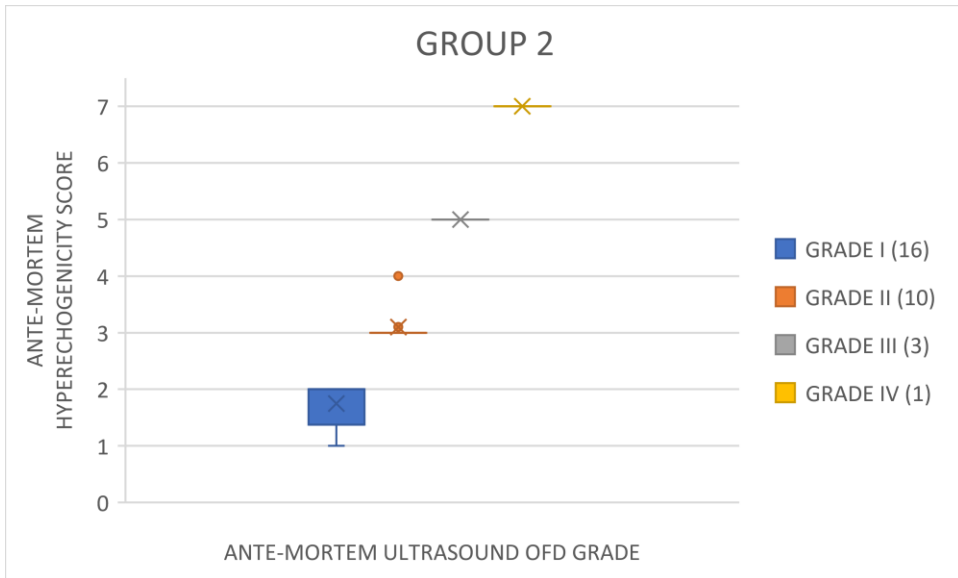


Figure 14. Graph illustrating the ante-mortem US hyperechogenicity scores and US OFD grades of ovaries in group 2.

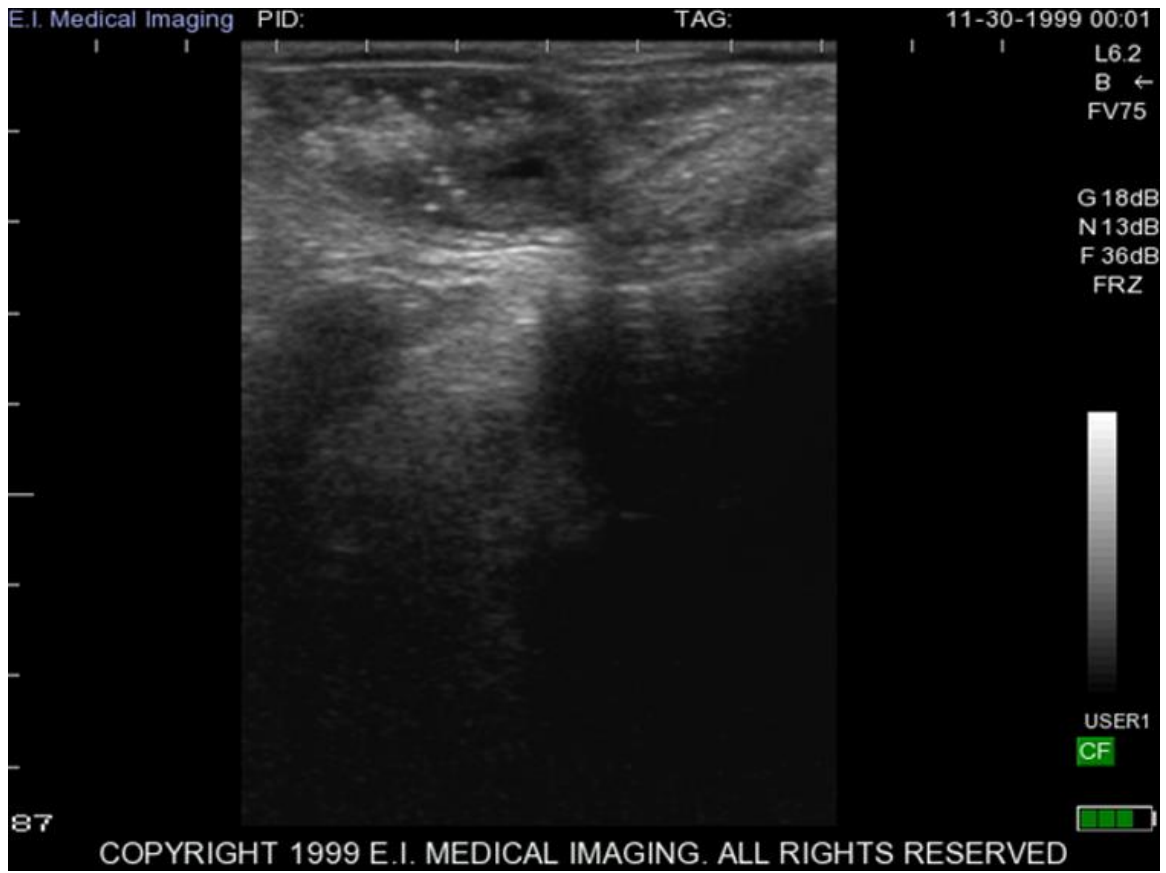


Figure 15. Trans-rectal ultrasound image of the right ovary taken ante-mortem. Multiple areas of hyperechogenicity are present in the ovary along with decreased numbers of Graafian follicles indicative of a grade IV ovarian follicular dysplasia cow.



Figure 16. Trans-rectal ultrasound image of the left ovary taken ante-mortem. There are multiple areas of hyperechogenicity and small cystic areas indicative of grade IV ovarian follicular dysplasia cow.

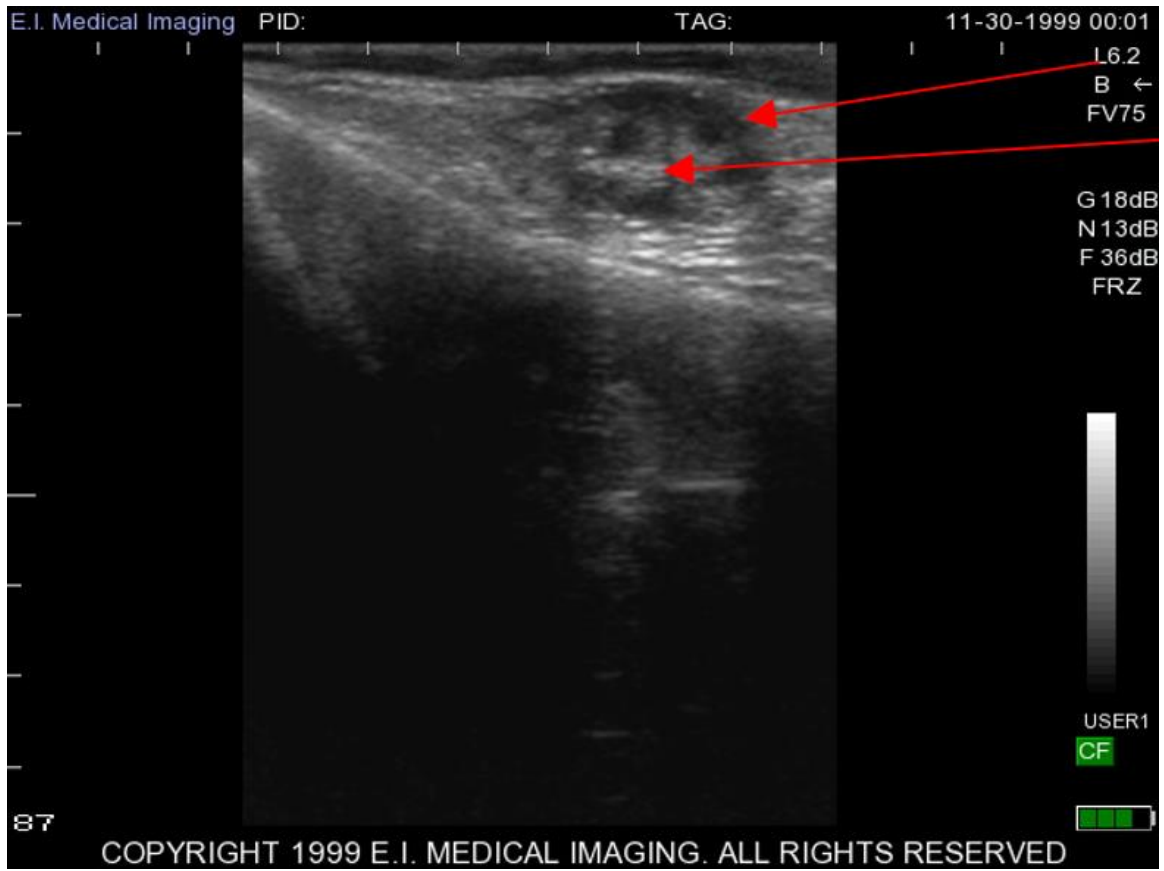


Figure 17. Trans-rectal ultrasound image of the ovary of a cow with grade II ovarian follicular dysplasia (OFD) taken ante-mortem. There are early cystic follicles (red arrows) with small areas of hyperechogenicity in the echoic rim. The cow was diagnosed with grade II OFD via trans-rectal ultrasound and was confirmed via histological analysis.

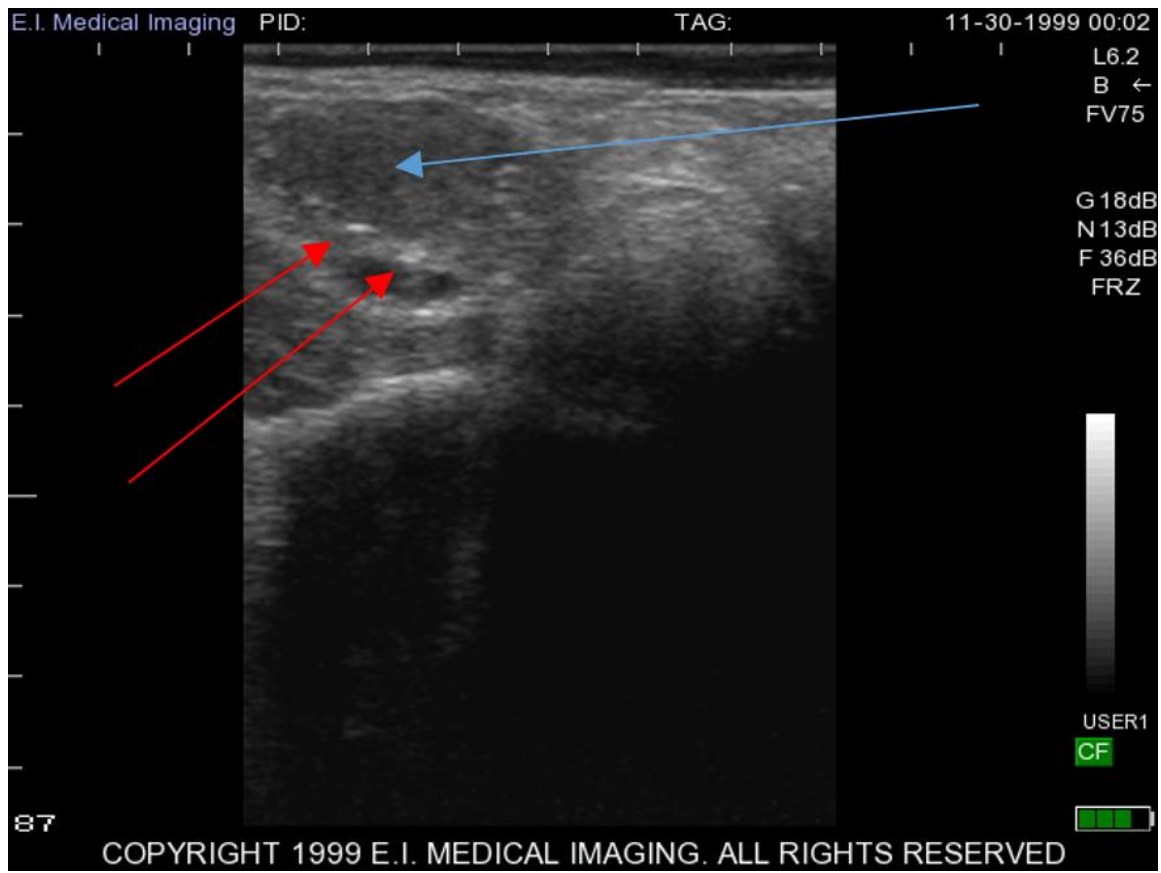


Figure 18. Ultrasound image of the ovary of a cow with grade II ovarian follicular dysplasia (OFD). There is a corpus luteum (blue arrow) with small areas of hyperechogenicity (red arrows). The cow was diagnosed with grade II OFD via ultrasound and was confirmed via histological analysis.

Increase in mineralization score via histology of OFD grade III was seen in this study as was reported in previous studies. Significant increases in mineralization occurred in grade III and IV OFD in comparison to OFD grades I and II and normal cattle (Roberts, 2017).

The agreement of trans-rectal ultrasonography compared to histologic examination of the ovaries for detection of OFD of cattle in group 1 (15 heifers) was 66.6% and in group 2 (15 cows) was 93.3% including histologically normal animals.

When comparing agreement ante-mortem ultrasound and histological analysis of diagnosis of the presence of OFD animals only, the agreement for group 1 was 71.4% and group 2 was 100%. Due to equipment malfunction and loss of data, the ante-mortem ultrasound images from group 3 were not available. The agreement of trans-rectal ultrasound and histology on the specific grade of OFD (I, II, III and IV) present in the ovaries in cattle in group 1 was 40% and in group 2 was 73.3%. Ultrasound examination found areas of hyperechogenicity on the four ovaries that were considered normal upon histological analysis. Hence, when including these ovaries in the overall agreement it was found that there was a 78.3% agreement between the ante-mortem (47/60) ovarian ultrasound and histological analysis of OFD in groups 1 and 2 (Figure 19). When the histologic normal ovaries were not included, there was a 83.9% agreement between ante-mortem ultrasound and histological analysis when combining groups 1 and 2. There was an 80% agreement between the post-mortem (24/30) ovarian ultrasound and histological diagnosis of OFD in groups 1, 2 and 3 including histologically normal ovaries (Figure 20). Removing the normal histological controls from the comparison then the agreement between post-mortem ultrasound and histology is 85.7%. In group 3, the agreement of post-mortem ultrasonography to histologic examination for detection of OFD was 60% (Figure 21). There was a higher number of ovaries called OFD positive when utilizing ultrasound in all groups that was detected on histologic analysis.

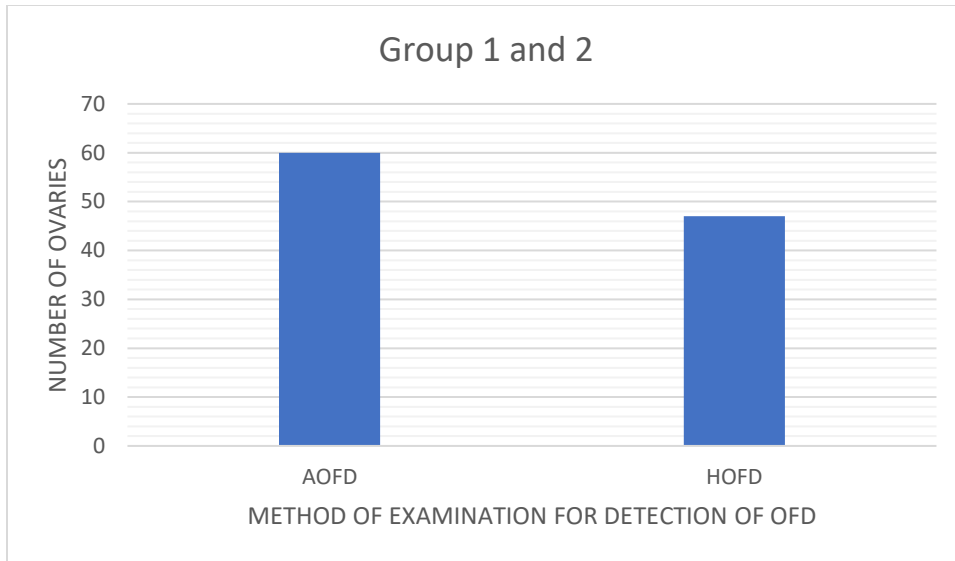


Figure 19. Graph illustrating the number of detected ovaries with OFD grades between ante-mortem US (AOFD) and histology (HOFD). Both methods of evaluation used 60 ovaries (from groups 1 and 2).

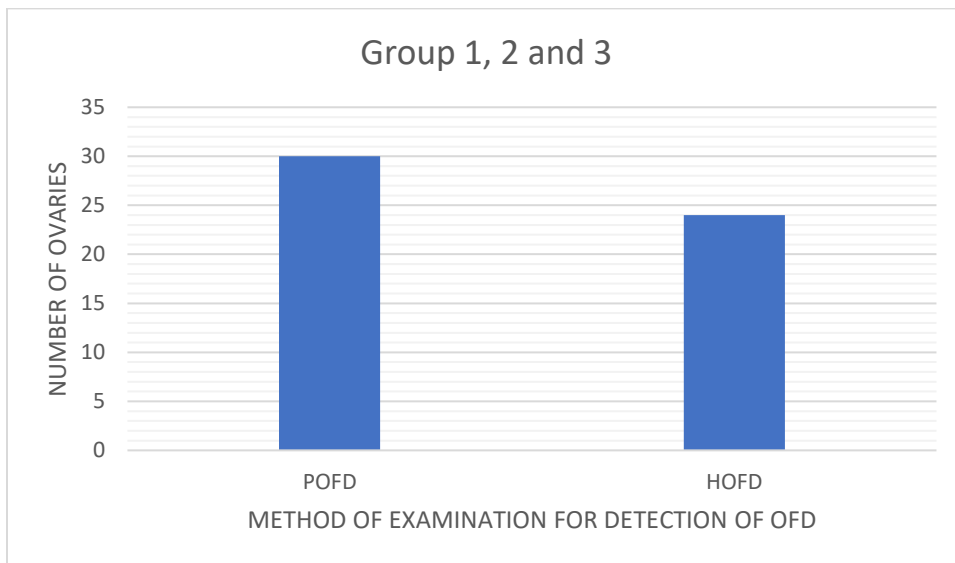


Figure 20. Graph illustrating the number of detected ovaries with OFD grades between post-mortem US (POFD) and histology (HOFD). Both methods of evaluation used 30 ovaries (from groups 1, 2 and 3).

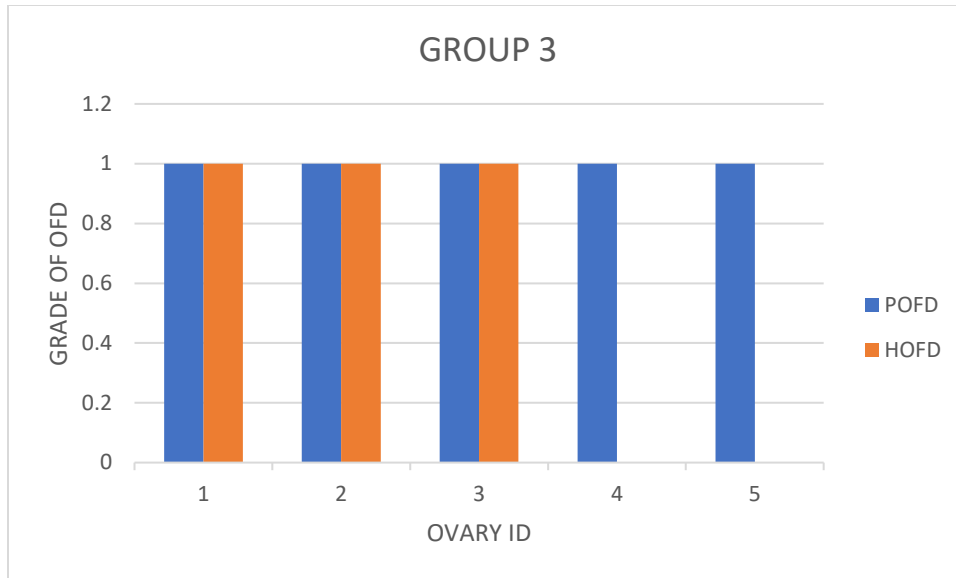


Figure 21. Graph illustrating the presence of OFD between post-mortem US (POFD) and histologic (HOFD) analysis of five ovaries from group 3.

The agreement of post-mortem ultrasonography compared to histologic examination for detection of OFD grades (I, II, and III) in group 1 was 40%, in group 2 was 6.6%, and group 3 was 60%.

There was 100% (25/25) agreement between the 7MHz ultrasound probe and the 8MHz ultrasound probe when evaluating ovaries for the presence of OFD in groups 1 and 2. The 8MHz machine had greater resolution, resulting in a higher OFD grade in 92% (23/25) of the ovaries versus that of the 7MHz ultrasound.

One ovary from each animal in Groups 1, 2 and 3 was also submitted for MRI. The evaluation of the MRI images was inconclusive for the presence of OFD. The scale utilized for ultrasound could not be applied to the MRI images due to difference in US image echogenicity and the MRI signal intensity. Some hyperechoic areas present within the ovaries on US were absent on the MRI images. Additional evaluations would be

necessary to determine any correlation between these imaging methods. However, antral follicle count (AFC) was performed. When the MRI AFC was compared to post-mortem ultrasound AFC, the population of antral follicles observed via MRI was two to three times (or more) greater than the AFC via ultrasound (Figures 22 to 25). Obviously, ultrasonography is less accurate when compared to MRI since ultrasound shows more of a two-dimensional picture and MRI is a stationary three dimensional image.

After MRI was performed, five ovaries from group 3 (one from each cow) were submitted for CT in an effort to more accurately determine the presence of dystrophic mineralization within the ovary. The CT results showed that 20% (1/5) of the ovaries contained areas of mineralized tissue as seen in the figure below (Figure 26 and 27).

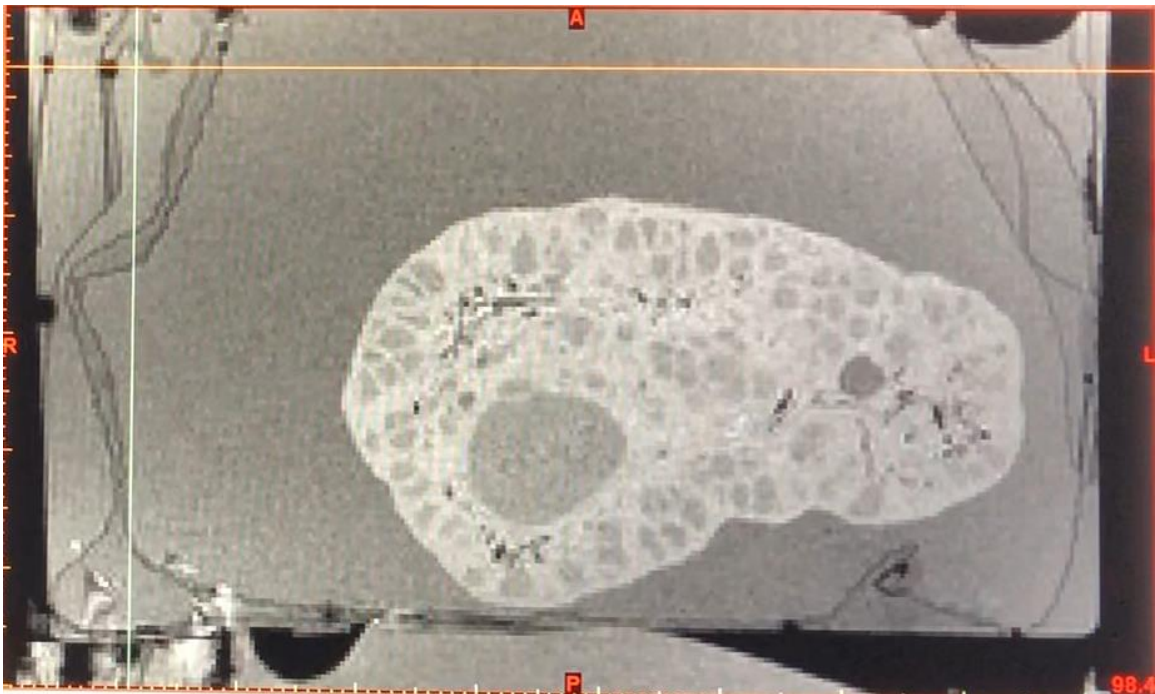


Figure 22. Ultrasound image of an ovary during MRI analysis. This ovary had OFD grade I OFD via histological analysis.



Figure 23. Image of MRI on five ovaries.

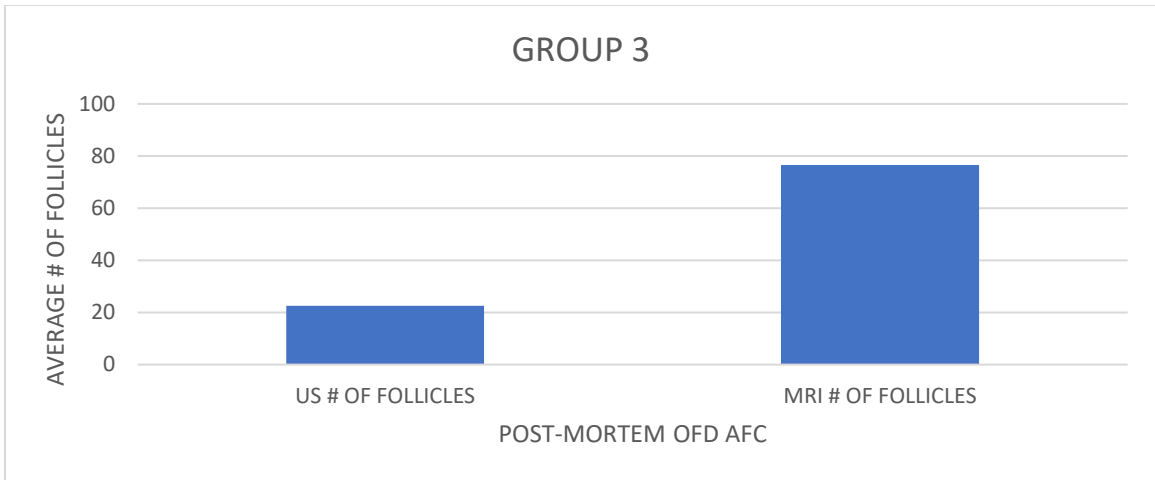


Figure 24. Graph illustrating the average numbers for antral follicle count (AFC) between post-mortem US and MRI evaluation of five ovaries from group 3.

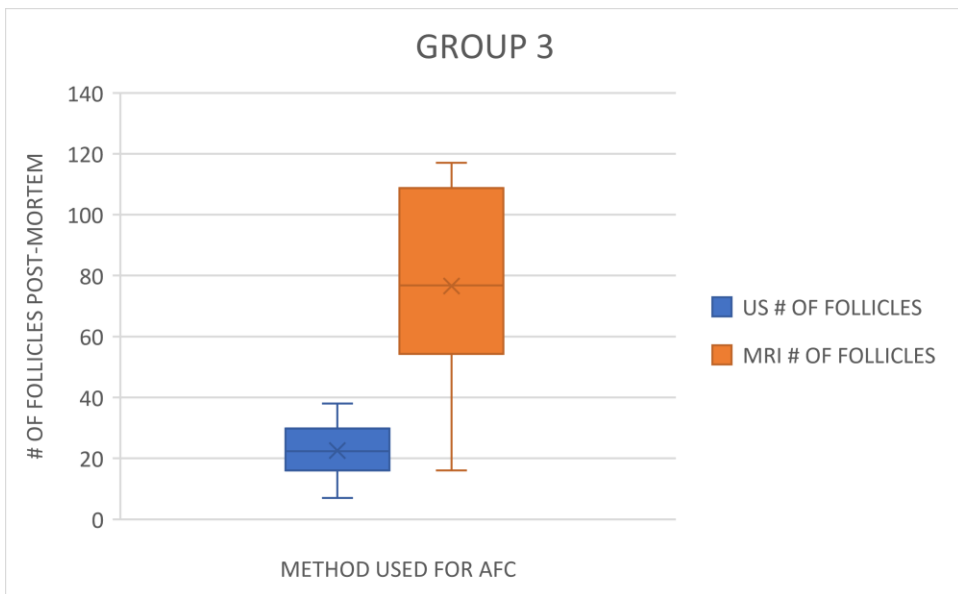


Figure 25. Graph illustrating the total numbers for antral follicle count (AFC) between post-mortem US and MRI evaluation of five ovaries from group 3.

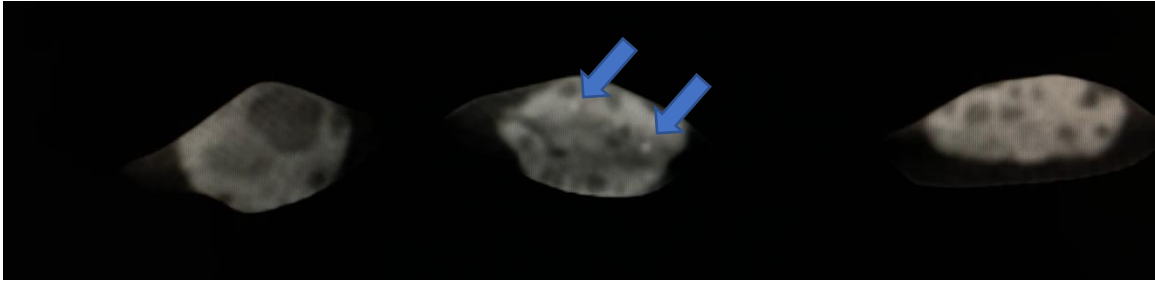


Figure 26. Three of the five ovaries evaluated via CT. The ovary located in the middle has two distinct mineralized areas (arrows). It was graded as OFD I via histology.

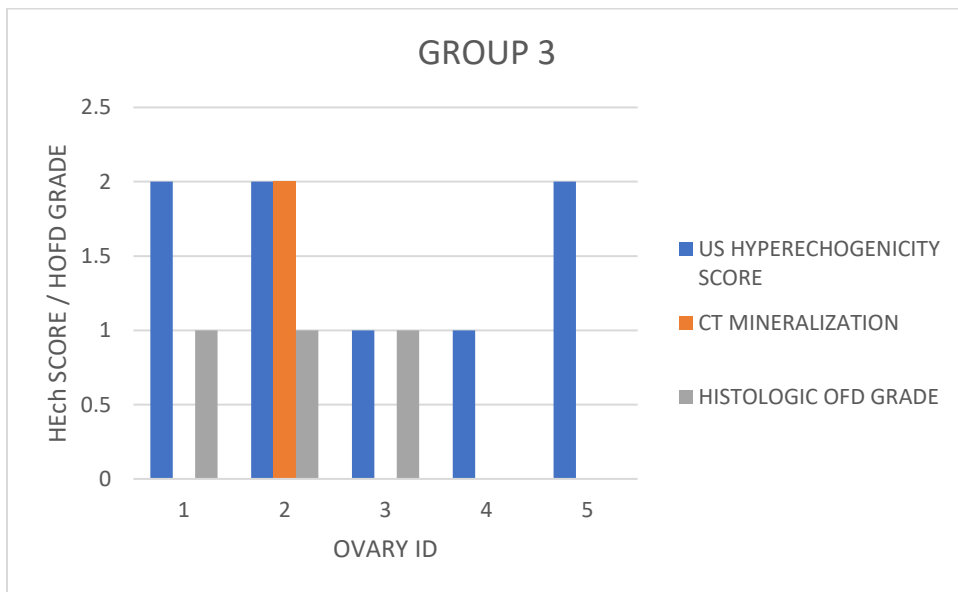


Figure 27. Graph illustrates the post-mortem US hyperechogenicity (HEch), degree of mineralization on CT and histologic OFD (HOFD) grade of ovaries from group 3.

The statistical analysis showed that the p-value for testing correlation of histological follicle number (HFol) and ante-mortem ultrasound follicle number (AFol) was found to be less than 0.05, therefore the correlation between HFol and AFol was

found to be statistically significant in group 1. The p-value for testing correlation of ante-mortem ultrasound hyperechogenicity grade (AHEch) and ante-mortem OFD grade (AOFD) was found to be less than 0.05, therefore the correlation between AHEch and AOFD was found to be statistically significant for group 2. The p-value for the testing correlation of ante-mortem ultrasound OFD grade (AOFD) and histologic OFD grade (HOFD) was found to be less than 0.05. Therefore, the correlation between AOFD and HOFD was statistically significant for group 2. The p-value for testing correlation of post-mortem ultrasound OFD grade (POFD) and histological OFD grade (HOFD) was found to be less than 0.05, therefore the correlation between POFD and HOFD was statistically significant for group 2. The p-value for testing correlation of post-mortem hyperechogenicity score (PHEch) and post-mortem OFD score (POFD) was less than 0.05, therefore the correlation between PHEch and POFD was found to be statistically significant. The p-value for testing correlation of AHEch and post-mortem hyperechogenicity (PHEch) was not less than 0.05, therefore the correlation between AHEch and PHEch was not statistically significant for group 2. The p-value for testing correlation of AOFD and POFD was not less than 0.05. Therefore, the correlation between AOFD and POFD was not statistically significant.

DISCUSSION

Cow longevity is a primary factor affecting profitability for cow-calf producers. Failure of cows and heifers to become pregnant is the primary reason a beef cow is removed from the production herd (Cushman et al, 2009). Management, environment, nutrition, and pathogens are some of the many factors that can negatively affect

pregnancy rates. The state of Florida has the lowest calf crop percentage, (76%) in the nation (Rae, 2010). Florida's calf crop is at least 10% lower than what is seen in other states (Rae, 2010). In the effort of trying to answer the questions of why Florida's calf crop is the lowest, OFD was discovered and was documented by Roberts (2008) in *Bos taurus x Bos indicus* cows. It has been stated that it is the leading cause of infertility in Florida beef cows (Buergelt et al, 2010; Roberts et al, 2016; Gard et al, 2016).

The results of a 2016-2018 study commissioned by the Florida Cattleman's Association found OFD to have an estimated prevalence ranging from 71.4% to 100% in animals from a variety of cull pens, in a subset of Florida ranches (Roberts et al, 2016). This study not only looked at prevalence of OFD in herds but laid the ground work for the identification of OFD via ante-mortem methods. Hence, ante-mortem ultrasound was utilized to capture images that might lead to early diagnosis of OFD within a herd.

Economically, infertility is devastating to producers and it has been estimated that for every percentage point of infertility within the herd there is an associated cost of \$11 per animal (Lamb, 2014). So, in Florida where the state's beef herd is approximately 1.69 million if 10% of the cows were affected by OFD, this translates to approximate losses of \$186 million/year in Florida alone (Livestock, 2015). From the two Florida ranches, histological analysis of the ovarian tissues from the culled cows indicated that OFD was diagnosed 80% of the time in cull animals, 10/15 (66.7%) and 14/15 (93%) in the first and second ranches, respectively (Roberts, 2017). The rates of OFD within these herds was consistent with what Roberts had found previously in Florida ranches (Roberts al., 2016). The number of heifers affected by OFD is quite staggering. It raises many questions. When and if the heifer calf is exposed in utero to toxins or viruses or if there is

a genetic predisposition within specific populations of cattle. Whatever the reason for the presence of OFD it is important to be able to detect affected animals and cull them from the herd. Reliable ante-mortem diagnosis is key to detection of OFD within a herd and will afford the ability of animals to be screened earlier in life and removed from the herd to reduce costs associated with rearing, housing and breeding them.

Ultrasound examination of the ovaries and the uterus was the ante-mortem test evaluated in this study. Ultrasound is convenient and non-invasive. It provides reliable information to the user, given that the user has been trained in rectal palpation and diagnostic ultrasound. Ultrasound is routinely utilized in determination of where the cow or heifer is in her cycle. It is used to determine structures on the ovary such as the presence or the absence of corpus lutea, follicles, atretic follicles, follicular and luteal cysts, and corpus hemorrhagica, Ultrasound can also detect changes in the density of the tissue within the ovary. Histological analysis is considered the gold standard for analysis of the ovary and any pathology within. Unfortunately, histological analysis can only be performed via an ovarian biopsy post surgically or post-mortem. Hence, use of a non-invasive tool like ante-mortem ultrasound is the least costly option for diagnosis of OFD. However, the reliability of ultrasound for diagnosis of OFD is not known. Therefore, this study was conducted to analyze the reliability of ultrasound in diagnosis of OFD.

Group 1 and 2 were cattle from within the state of Florida. Group 3 was added to have a group of cattle that were clinically reproductively normal located outside the state of Florida to use as a normal control. Since histological results showed three out of five animals positive for OFD, this objective was not achieved but these animals were still included in the project for a potentially better understanding of OFD. It seems that cattle

with lower grades of OFD can still be reproductively functional like those in group 3. However, this cannot be said with all cows or heifers with lower grades of OFD as seen in the Florida population where the animals were not fertile. It might be that there are normal aging changes that go on within the ovary that overlap with what is seen in cattle with OFD both histologically and via ultrasound as well.

When the ante-mortem and post-mortem ultrasound results were compared with histological analysis, there was a higher agreement between ante-mortem ultrasonography and histology grades. This correlation may be related to the amount and location of ovarian area analyzed in both exams. Since the ante-mortem ultrasound evaluation was based on one image of the largest dimension of the ovaries, the chances are good that the histological sample and the ante-mortem images were the same or a similar area. So, it was more expected that the ante-mortem ultrasound including hyperechogenicity scoring, and follicular counts as well as OFD scoring is correlated with histological analysis and detection of OFD.

It is important to remember that in the post-mortem ultrasound examination, whole ovaries were analyzed in several videos from different angles. The increase in OFD grades in post-mortem ultrasonography is therefore believed to be related to the greater ovarian volume examined. Thus, the greater extent of examination, the higher the incidence of hyperechogenicity found within the ovaries, and the higher the US OFD grades. There was also a higher post-mortem ultrasound OFD grading in group 1, which was composed exclusively of heifers. This may mean that there is an increase in the follicular activity and shorter cycle length resulting in areas in the ovary that have increase rates of development and so may appear more dense than other areas. However,

there also could be areas within the ovary that do not produce normal follicles and those follicles become non-responsive and may never ovulate and/or do not undergo atresia normally.

What these hyperechogenic areas represent as far as ovarian structures has not been completely defined, but they have ultrasonographic characteristics of mineralization, fibrosis, abscessation and/or possibly adipose tissue. Further analyzes are needed to identify the nature of these structures. Additional special staining for extracellular matrix and immunohistochemistry for smooth muscle would be useful for analysis of ovarian stroma. We do know histologically that dystrophic mineralization occurs in malformed follicles within the ovary as seen with Grade III and IV OFD (Roberts 2016). If there are numerous areas which have dystrophic mineralization and/or degenerate follicles with mineralization, this may result in dense areas having mineral within the ovary and are hyperechoic upon ultrasound examination. The hyperechoic tissue may also be dense fibrotic tissue that is nonfunctional, similar to what is seen with testicular fibrosis. However, dense areas of purulent material can also look hyperechoic on ultrasound, but this has not been seen on ovaries with OFD. The additional staining procedures and or micro-CT would help answer these questions concerning hyperechogenic areas within the ovary.

The amount of data collected for histological analysis (from one section) and ante-mortem ultrasound examination (from one image) lead us to believe that we may have been under-diagnosing the presence of OFD and even it's grades. On the other hand we may be seeing a variation of normal and not realize that the ultrasound is compounding the densities of the tissues throughout the ovary resulting in an error in our

interpretation of the ultrasound screen. For future studies, it may be valid to suggest that grading ovarian mineralization, fibrosis, abscessation and adipose tissue, and performing multiple sections for histology might give more information prior to grading OFD so that a more complete picture is seen of the ovary.

The antral follicular count (AFC) of the animals from Florida and Alabama varied from animal to animal. The AFC tends to be variable between different animals but has high repeatability within individuals (Morotti et al, 2017). In a review article by Morotti in 2017, he compares articles about AFC between *Bos t. taurus* versus *Bos t. indicus*. His conclusion was that larger numbers of follicles, better quality embryos, better pregnancy rates, increased concentrations of circulating P4 and other characteristics linked to fertility are all characteristics associated with animals with high AFC, compared to those with low AFC in *Bos t. taurus*. On the contrary, in *Bos t. indicus* the association between high AFC and fertility did not follow the same pattern. Recent studies showed no association between fertility and AFC for Zebu cattle (Morotti et al, 2017). In this study, MRI was a much more reliable indicator of true AFC than ultrasound. MRI provides a much more accurate picture of AFC because it is a 3D view of the ovary. Ultrasound is more of a 2D view of the ovary and often times a person may think that they are ultrasounding the same follicles when in reality they may be seeing additional follicles and not counting them when they should. The cow moves, the probe moves, the picture changes, and this can lead to alterations in getting as accurate count of the follicles, as seen in this study.

From the MRI and CT data of the ovaries, we have concluded that for future studies, micro CT may be a better choice for collection and analysis of data regarding

AFC, mineralization, fibrosis, abscessation, adipose tissue, CLs, ovarian stroma, and vessels. Micro CT has the ability to distinguish regions of ovarian cortex and medulla, visualize the morphology and distribution of blood vessels, observe corpus luteum and antral follicles, and even detect oocytes inside some antral follicles (Paulini et al, 2016).

In summary, OFD often has the clinical presentation as a repeat breeder, but mucometra, aseptic metritis, abortion and early embryonic death may all be seen. The higher grades of OFD (Grades III and IV) can be detected by ultrasound mainly based on visualization of severe dystrophic mineralization and cystic structures. The ability to detect these grades of OFD in animals ante-mortem is important as these are the severe cases can alert the producer to a reproductive problem in the herd. There remain many questions surrounding OFD. It is believed that OFD is not associated with any known infectious agent. Ovarian follicular dysplasia is a slowly progressive, (“lifelong”), bilateral ovarian follicle dysplasia that eventually transforms into bilateral benign Sertoli-form-Granulosa cell tumor. The etiology of this condition is still unknown and further studies are needed for a better understanding of the causes and consequences of OFD.

CONCLUSIONS

The results of this study showed a correlation between the presence of one or more hyperechogenic areas within ovaries, on ultrasound images, and the presence of OFD in those ovaries according to histologic evaluation. The authors concluded that the increase in echogenicity on US images within the ovary was abnormal and suggestive for presence of OFD. The correlation between ante-mortem US examination and histologic evaluation for the presence of OFD in the ovary was between 66.6% and 93.3%, and 80%

when groups 1 and 2 were combined. Most of the disagreement was found with calling an ovary OFD grade I that was histologically found to be normal, type I error. If the OFD grade I's were removed from this analysis, then there would be 100% agreement between ultrasound and histology for diagnosis of OFD. The discrepancy between ultrasound grading and histological grading is based on a number of important factors such as amount of ovary evaluated, microscopic versus macroscopic (gross) analysis, and interpretation of what the hyperechogenicity represents. The ultrasound picture can be misleading because of the various angles and the density of the tissues is compounded throughout the ovary. Additional studies are necessary to determine the tissues leading to the hyperechoic areas within the ovary. More comparison studies are needed between histology, ultrasound, MRI and micro-CT to fully elucidate the connection between histological analysis and ultrasound.

Also, the difference between 7MHz (ante-mortem US) and 8MHz (post-mortem US) probes' did not affect the results of this study and both correlated with histological detection of OFD. This study also showed a correlation between ante-mortem and post-mortem US AFC and US HEch as well as a correlation between US AFT and MRI AFT. Trans-rectal ultrasound is a reliable tool to diagnose OFD ante-mortem.

REFERENCES

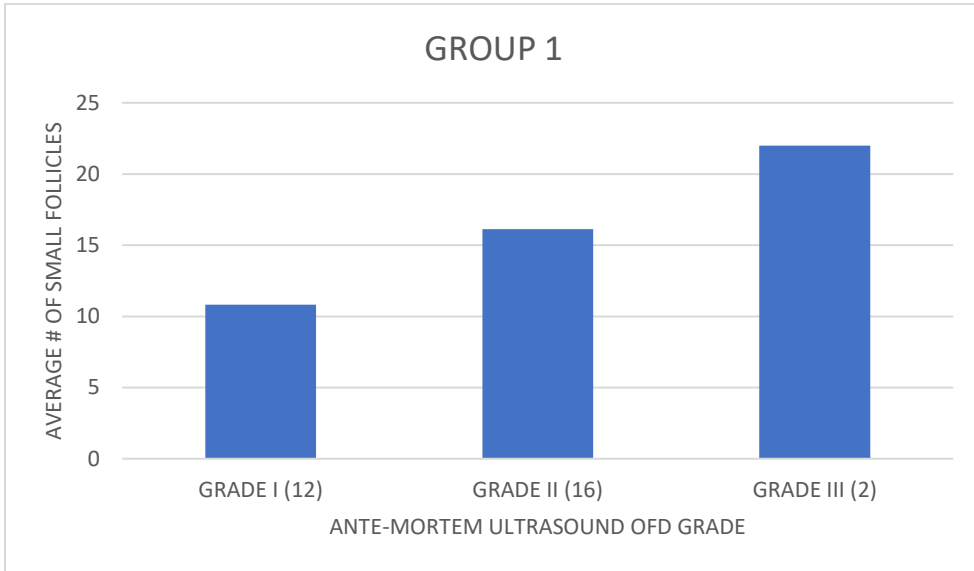
- (2016, June 1). Florida - **Livestock** - Dairy and Poultry Summary - 2015. *USDA, National Agricultural Statistics Service*. Retrieved August 13, 2016, from https://www.nass.usda.gov/Statistics_by_State/Florida/Publications/Livestock_and_Poultry/.
- Andersen, C. Y.,** Baltsen, M., & Byskov, A. C. (1999). Gonadotropin-Induced Resumption of Oocyte Meiosis and Meiosis-Activating Sterols, *41*, 163-185. Retrieved January 11, 2019, from 10.1016/s0070-2153(08)60273-2.
- Baba, A. I. & Cătoi, C.** (2007). *Comparative Oncology*. The Publishing House of the Romanian Academy. Bookshelf ID: NBK9555.
- Beker van Woundenberg, A. R. C. L.** (2004). *Fundamental aspects of bovine oocyte maturation: The role of estradiol, VIP and GNRH*. Utrecht, Netherlands.
- Britt, J. H.** (2008). Oocyte development in cattle: physiological and genetic aspects. *R. Bras. Zootec.*, *37*(spe), 110-115. Retrieved February 3, 2019, from 10.1590/s1516-35982008001300013.
- Buergelt, C. D.** (1997). *Color atlas of reproductive pathology of domestic animals* (pp. 100-111). St. Louis: Mosby Incorporated.
- Buergelt, C.,** Heskett, T., Roberts, J., & Irsik, M. (2010). Ovarian dysplasia and neoplasia as cause of culling beef cattle in southern Florida. (p. 1023). Presented at the World Buiatrics Conference Proceedings.
- Capel, B.** (1996). The Role of Sry in Cellular Events Underlying Mammalian Sex Determination, 1-37. Retrieved December 15, 2018, from 10.1016/s0070-2153(08)60423-8.
- Cushman, R. A.,** Allan, M. F., Kuehn, L. A., Snelling, W. M., Cupp, A. S., & Freetly, H. C. (2009). Evaluation of antral follicle count and ovarian morphology in crossbred beef cows: Investigation of influence of stage of the estrous cycle, age, and birth weight^{1,2}, *87*(6), 1971-1980. Retrieved January 6, 2019, from 10.2527/jas.2008-1728.
- Dyce, K.,** Sack, W., & Wensing, C. (2010). *Textbook of Veterinary Anatomy* (4th ed., p. 701). St. Louis, Missouri: Saunders, an imprint of Elsevier Inc.

- Fricke, P., & Lamb, G. (2002).** Practical Applications of Ultrasound for reproductive Management of Beef and Dairy Cattle. In. Presented at the The Applied Reproductive Strategies in Beef Cattle Workshop, Manhattan, Kansas. Retrieved October 12, 2018, from https://beefrepro.unl.edu/proceedings/2002manhattan/18_ksu_usound_lambfricke.pdf
- Gard, J. (2003, December 19).** *Infectivity of Bovine Viral Diarrhea Virus Associated with in vivo Derived Bovine Embryos* (PhD dissertation). Auburn University, Auburn, Alabama.
- Gard, J. A., Roberts, J., Braden, T., Mansour, M., Yelich, J., Irsik, K., Rae, O., & Wenzel, J. G. (2017).** Assessment of ovarian follicular dysplasia utilizing ultrasound and histologic examination. *Reprod. Fertil. Dev.*, 29(1), 168. Retrieved January 7, 2019, from 10.1071/rdv29n1ab119
- Ginther, O. J. (1995).** *Ultrasonic imaging and animal reproduction* (p. 7). Cross Plains, WI, USA.
- Ginther, O., Wiltbank, M., Fricke, P., Gibbons, J., & Kot, K. (1996).** Selection of the dominant follicle in cattle. *Biol Reprod.*, (55), 1187-94.
- Hafez, E. S., & Hafez, B. (2000).** *Reproduction in Farm Animals* (7th ed., pp. 68-91). Lippincott Williams & Wilkins.
- Hastie, N. D. (1992).** Dominant negative mutations in the Wilms tumour (WT1) gene cause Denys-Drash syndrome—proof that a tumour-suppressor gene plays a crucial role in normal genitourinary development. *Hum Mol Genet.*, 1(5), 293-295. Retrieved December 11, 2018, from 10.1093/hmg/1.5.293.
- Hunt, P., & LeMaire-Adkins, R. (1997).** Genetic Control of Mammalian Female Meiosis, 37, 359-381. Retrieved February 12, 2019, from 10.1016/s0070-2153(08)60180-5
- Johnson, J., Canning, J., Kaneko, T., Pru, J., & Tilly, J. (2004).** Germline stem cells and follicular renewal in the postnatal mammalian ovary. *Nature.*, (428), 145-150. Retrieved February 7, 2019, from <https://www.nature.com/articles/nature02316>

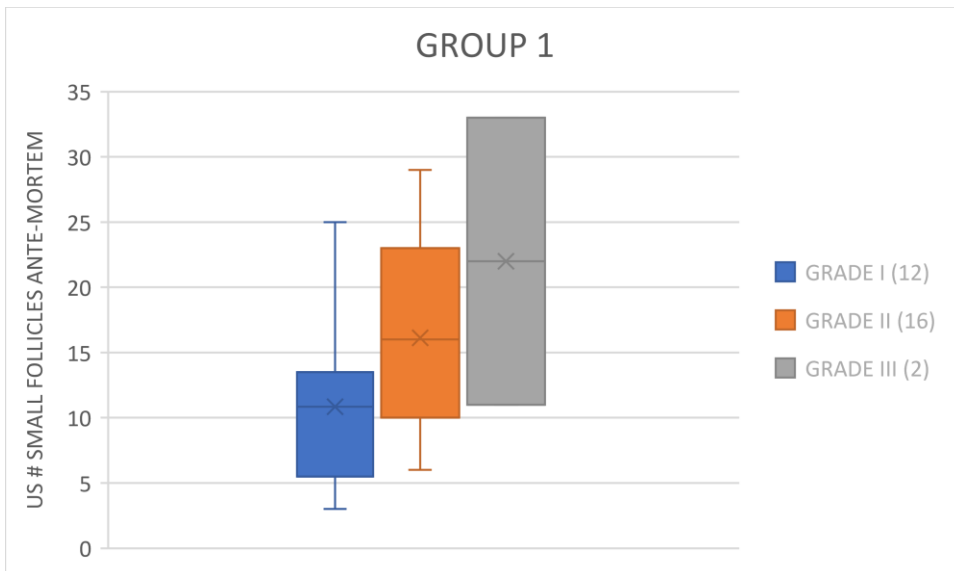
- Küber, H., & Jalakas, M. (2002).** Pathological Changes in the reproductive organs of Cows and Heifers Culled because of Infertility. *J Vet Med A Physiol Pathol Clin Med*, (49), 365-72.
- Lamb, C., Dahlen, C., Mercadante, V., & Bischoff, K. (2014).** What is the impact of infertility in beef cattle? In *IFAS Extension, Unive. of FL, AN208*. Gainesville, Florida. Retrieved January 7, 2019, from <https://edis.ifas.ufl.edu/an208>
- Landim-Alvarengal, F., & Maziero, R. (2014).** Control of oocyte maturation. *Anim. Reprod.*, 11, n.3(Jul./Sept), 150-58. Retrieved January 7, 2019, from <https://pdfs.semanticscholar.org/eb45/30356be972684afca53cfeaddb9bf889c95d.pdf>
- Morotti, F., Zangirolamo, A., Silva, N., Silva, C., Rosa, C., & Seneda, M. (2017).** Antral follicle count in cattle: advantages, challenges, and controversy. In *Proceedings of the 31st Annual Meeting of the Brazilian Embryo Technology Society*. Cabo do Santo Agostinho, Brazil.
- Naillat, F., Yan, W., Karjalainen, R., Liakhovitskaia, A., Samoylenko, A., Xu, Q., Sun, Z., Shen, B., Medvinsky, A., & Quaggin, S. (2015).** Identification of the genes regulated by Wnt-4, a critical signal for commitment of the ovary. *Experimental Cell Research*, 332(2), 163-178. Retrieved April 4, 2019, from 10.1016/j.yexcr.2015.01.010
- Norris, H., Taylor, H., & Garner, F. (1969).** Comparative Pathology of Ovarian Neoplasms. *Path Vet*, 6, 45-58. Retrieved January 6, 2019, from <https://journals.sagepub.com/doi/pdf/10.1177/030098586900600104>
- Paulini, F., Chaves, S. B., Rolo, J. L. J., Azevedo, R. B. D., & Lucci, C. M. (2019).** Evaluation of ovarian structures using computerized microtomography. *An. Acad. Bras. Ciênc.*, 89(3 suppl), 2131-2139. Retrieved November 18, 2018, from 10.1590/0001-3765201720150864
- Parker, K. L., Schimmer, B. P., & Schedl, A. (1999).** Genes essential for early events in gonadal development. *CMLS, Cell. Mol. Life Sci.*, 55(7), 831. Retrieved November 11, 2018, from 10.1007/s000180050337

- Pierson, R., & Ginther, O. (1988).** Ultrasonic imaging of the ovaries and uterus in cattle. *Theriogenology*, 29, 21-37. Retrieved December 7, 2018, from <https://www.sciencedirect.com/science/article/pii/0093691X88900295>
- Rae, D. (2006, June 30).** Raising the calf crop in Florida beef cattle. Retrieved April 16, 2019, from <https://re eis.usda.gov/web/crisprojectpages/0185634-raising-the-calf-crop-in-florida-beef-cattle.html>
- Roberts, J., Irsik, K., Swain, H., Lollis, G., Kitchen, D., Stockdale, H., Morales, O., Buergelt, C., Schlafer, D., & Austin, B. (2008).** Reproductive tract examination at slaughter of repeat breeding beef cows and heifers in south central Florida. In. Presented at the AAVLD, 51st Annual conf., Greensboro, North Carolina.
- Roberts, J., Steel, E., Gard, J., Yelvington, J., Siegel, N., Hinds, J., Freel, W., Armstrong, C., Hardee, I., & Rae, O. (2016).** Morphological characteristics of Ovarian Follicular Dysplasia (OFD) observed by ultrasound in four Florida beef herds. *Clinical Theriogenology*, 8, 325.
- Schatten, H., & Constantinescu, G. (2007).** *Comparative Reproductive Biology* (p. 41). Blackwell.
- Senger, P. (2012).** *Pathways to Pregnancy and Parturition* (3rd ed., Chapter 2: pp. 11-41). Redmond, Oregon: Current Conceptions, Inc.
- Senger, P. (2012).** *Pathways to Pregnancy and Parturition* (3rd ed., Chapter 4: pp. 81-97). Redmond, Oregon: Current Conceptions, Inc.
- Senger, P. (2012).** *Pathways to Pregnancy and Parturition* (3rd ed., Chapter 8: pp. 161-177). Redmond, Oregon: Current Conceptions, Inc.
- Senger, P. (2012).** *Pathways to Pregnancy and Parturition* (3rd ed., Chapter 9: pp. 181-200). Redmond, Oregon: Current Conceptions, Inc.
- Shahrokhi, S. Z., Kazerouni, F., & Ghaffari, F. (2018).** Anti-Müllerian Hormone: genetic and environmental effects. *Clinica Chimica Acta*, 476, 123-129. Retrieved April 2, 2019, from 10.1016/j.cca.2017.11.027
- Whitaker, M. (1996).** Control of meiotic arrest. *Reviews of Reproduction*, 1(2), 127-135. Retrieved January 11, 2019, from 10.1530/revreprod/1.2.127.

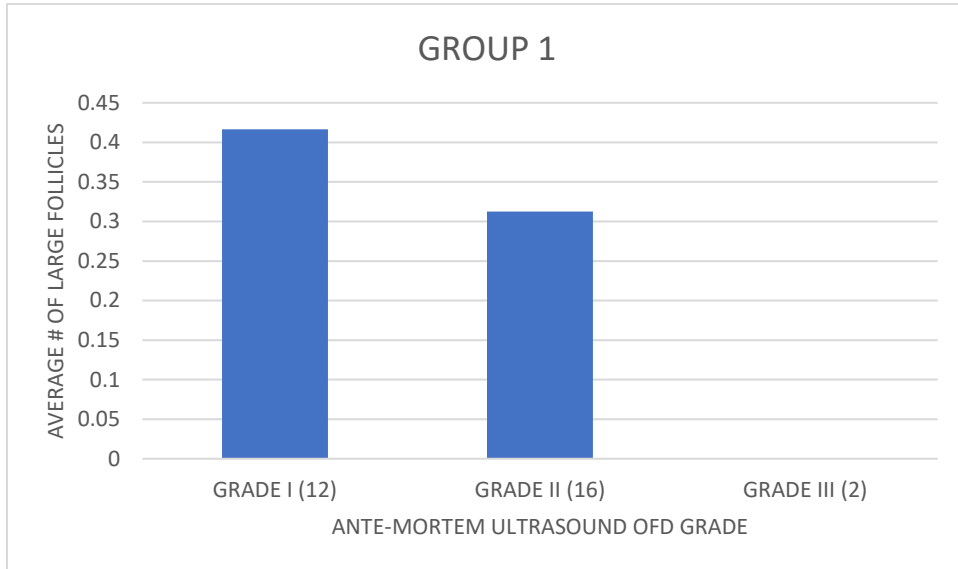
Appendix 1 – Graph illustrating the average of ante-mortem antral follicle count (AFC) number of small follicles (<4mm) in ovaries with US OFD grades I, II and III from group 1.



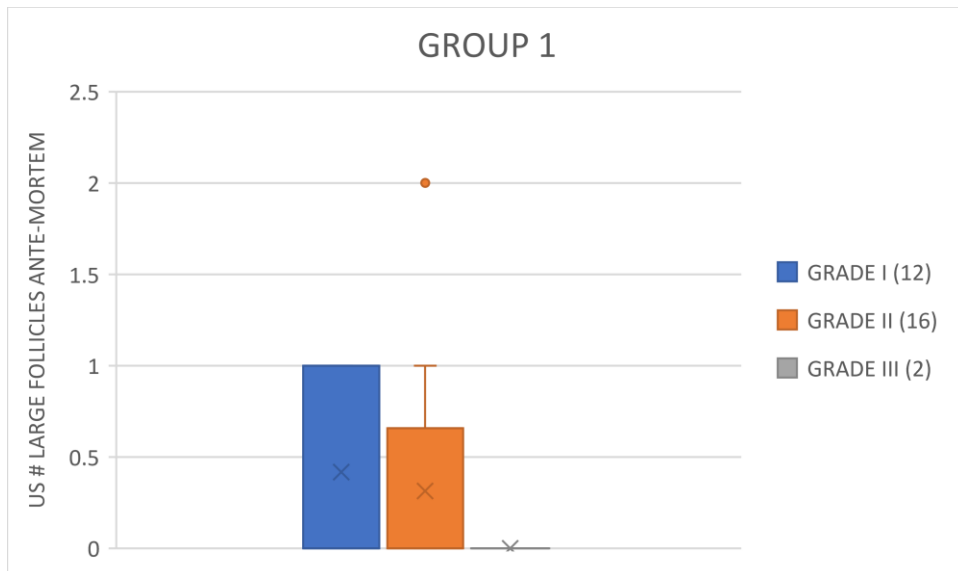
Appendix 2 - Graph illustrating the ante-mortem antral follicle count (AFC) numbers of small follicles (<4mm) in ovaries with US OFD grades I, II and III from group 1.



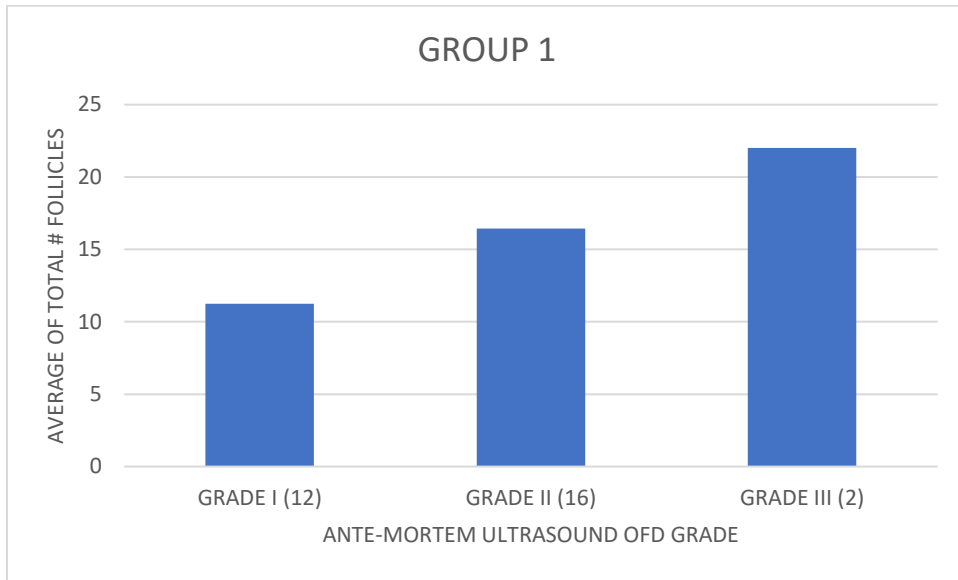
Appendix 3 - Graph illustrating the average of ante-mortem antral follicle count (AFC) numbers of large follicles ($\geq 5\text{mm}$) in ovaries with US OFD grades I, II and III from group 1.



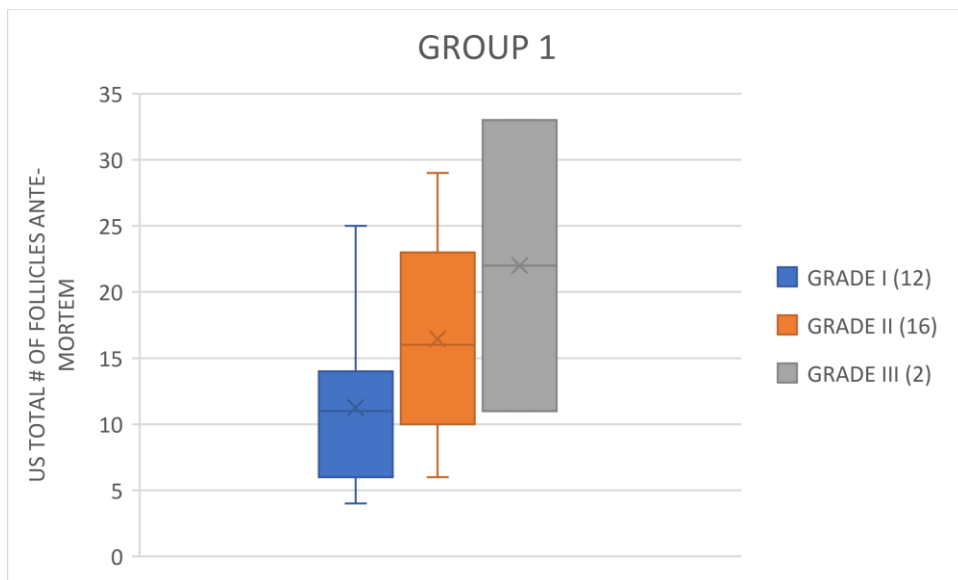
Appendix 4 - Graph illustrating the ante-mortem antral follicle count (AFC) numbers of large follicles ($\geq 5\text{mm}$) in ovaries with US OFD grades I, II and III from group 1.



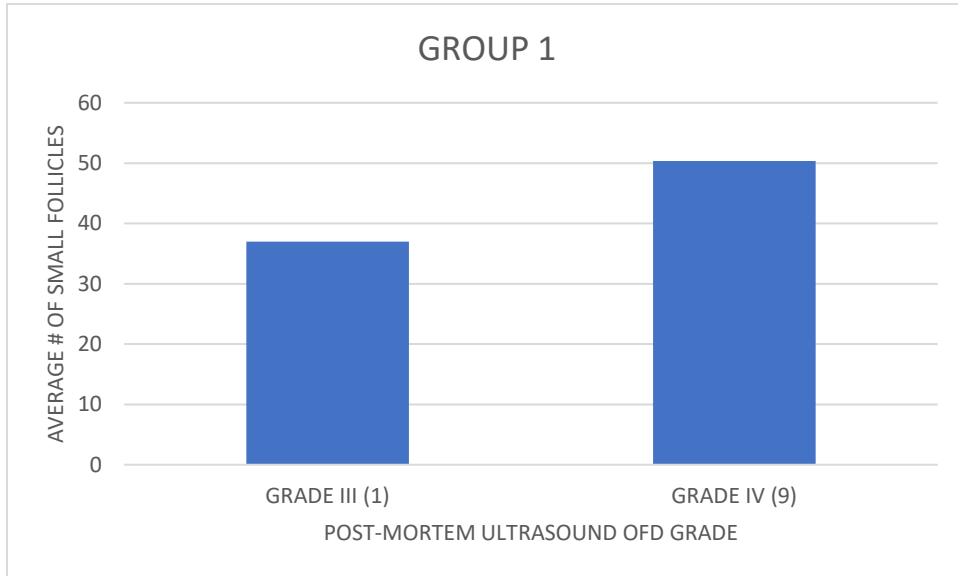
Appendix 5 - Graph illustrating the average number of ante-mortem antral follicle count (AFC) in ovaries with US OFD grades I, II and III from group 1.



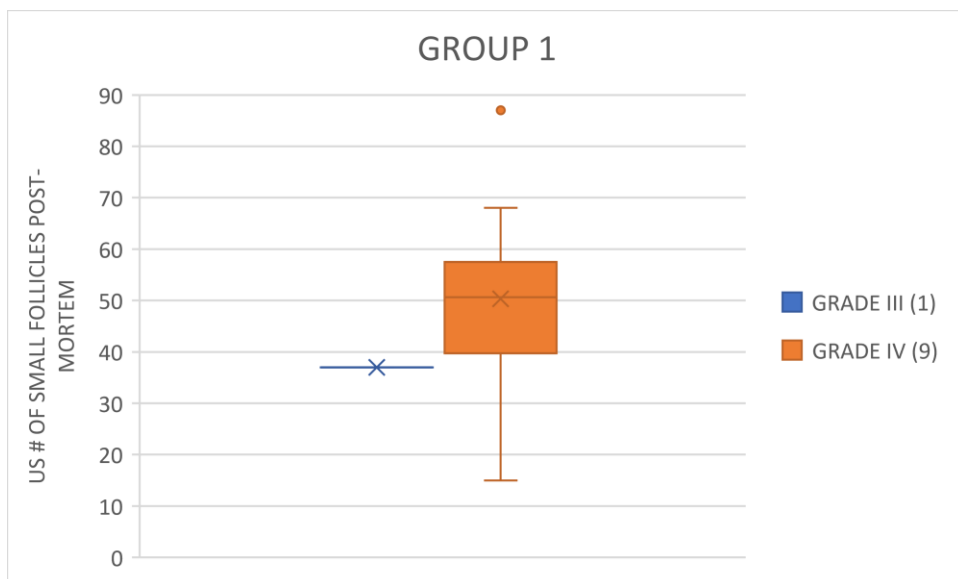
Appendix 6 - Graph illustrating the number of ante-mortem antral follicle count (AFC) in ovaries with US OFD grades I, II and III from group 1.



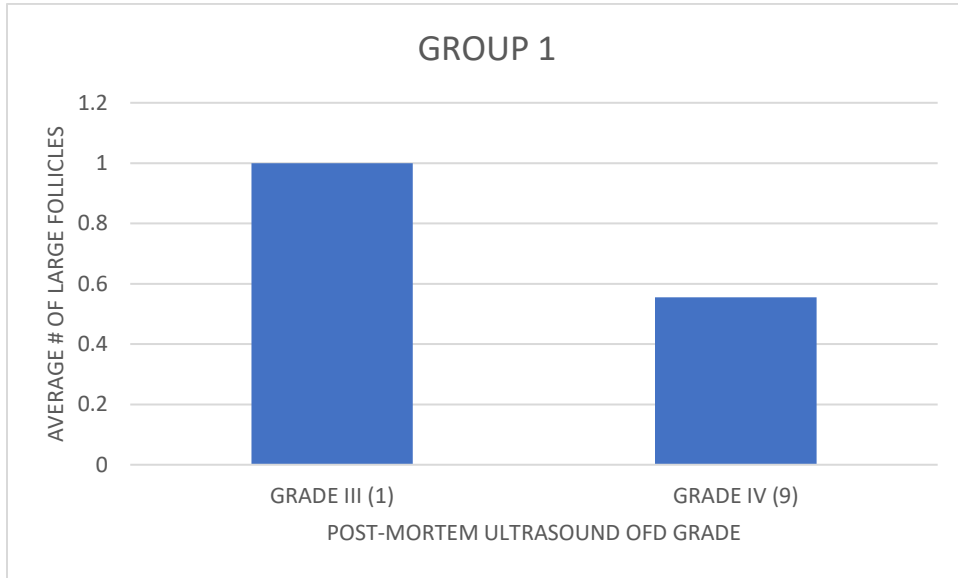
Appendix 7 - Graph illustrating the average of post-mortem antral follicle count (AFC) numbers of small follicles (<4mm) in ovaries with US OFD grades III and IV from group 1.



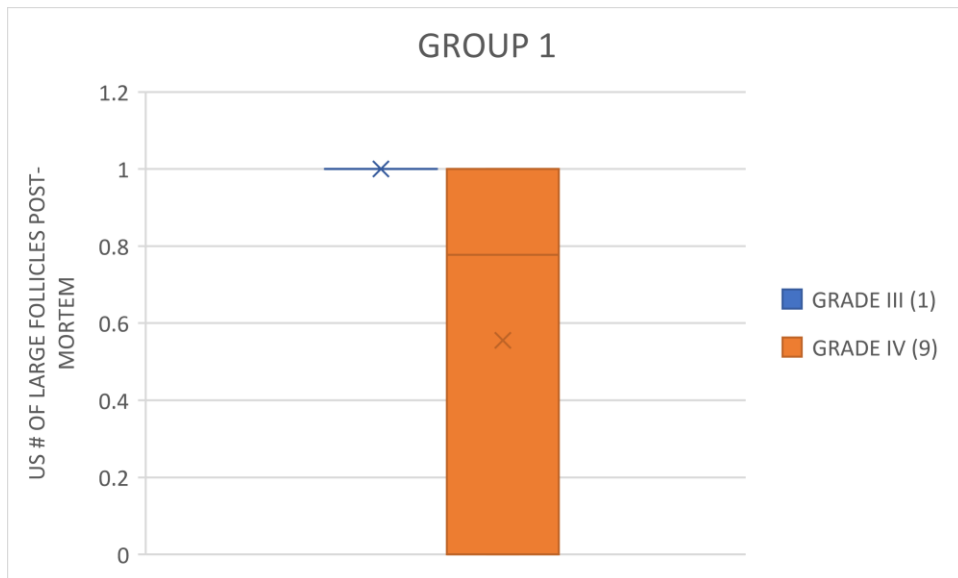
Appendix 8 - Graph illustrating the numbers of post-mortem antral follicle count (AFC) numbers of small follicles (<4mm) in ovaries with US OFD grades III and IV from group 1.



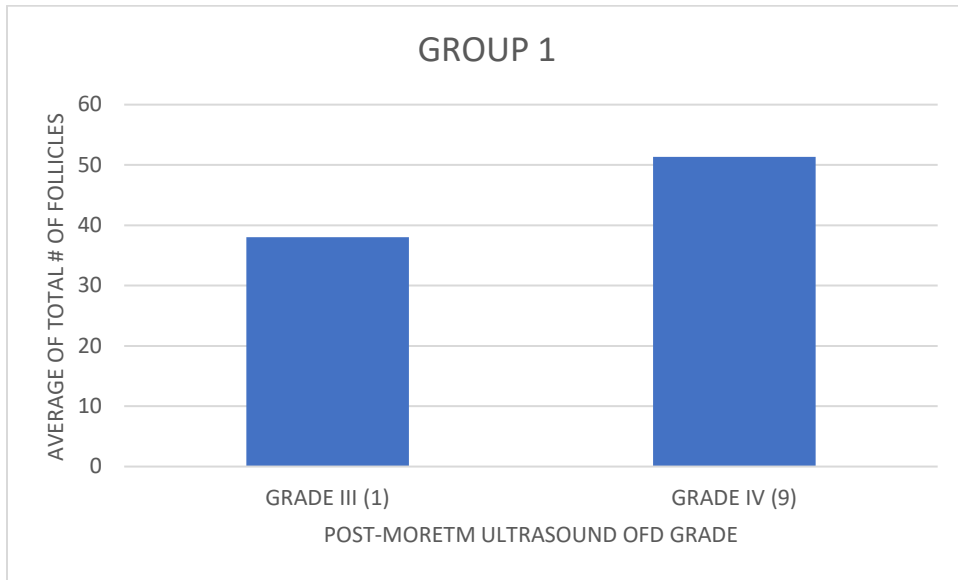
Appendix 9 - Graph illustrating the average of post-mortem antral follicle count (AFC) numbers of large follicles ($\geq 5\text{mm}$) in ovaries with US OFD grades III and IV from group 1.



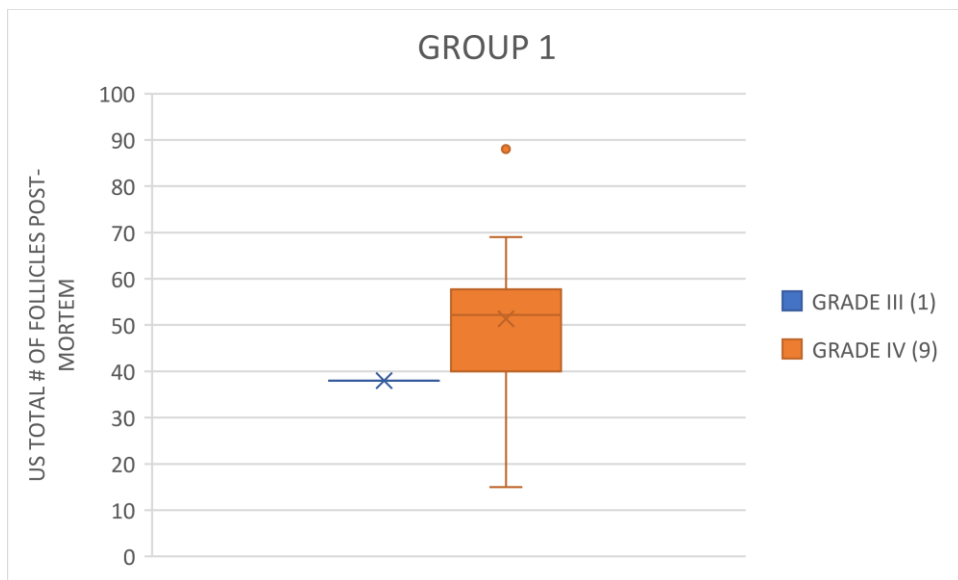
Appendix 10 - Graph illustrating the post-mortem antral follicle count (AFC) numbers of large follicles ($\geq 5\text{mm}$) in ovaries with US OFD grades III and IV from group 1.



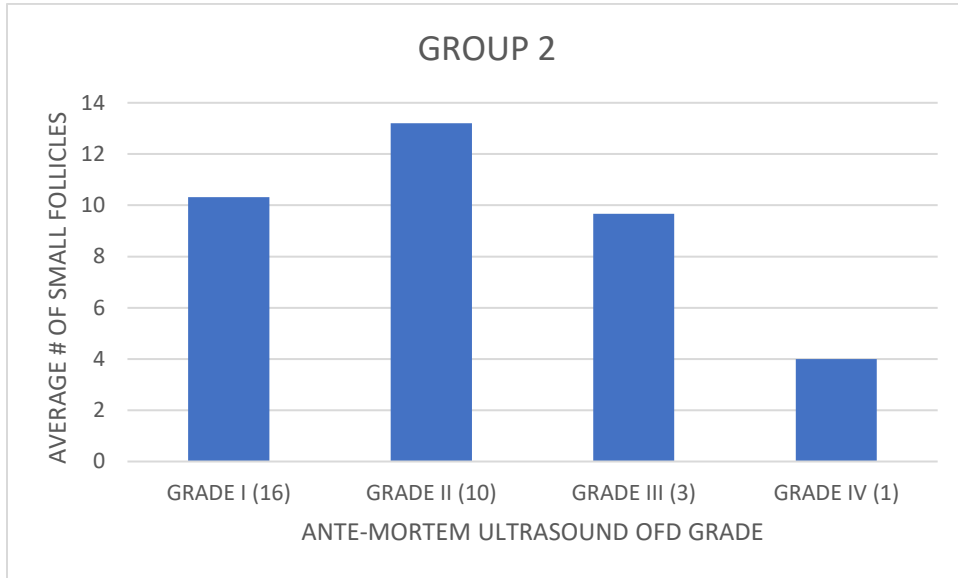
Appendix 11 - Graph illustrating the average number of post-mortem antral follicle count (AFC) in ovaries with US OFD grades III and IV from group 1.



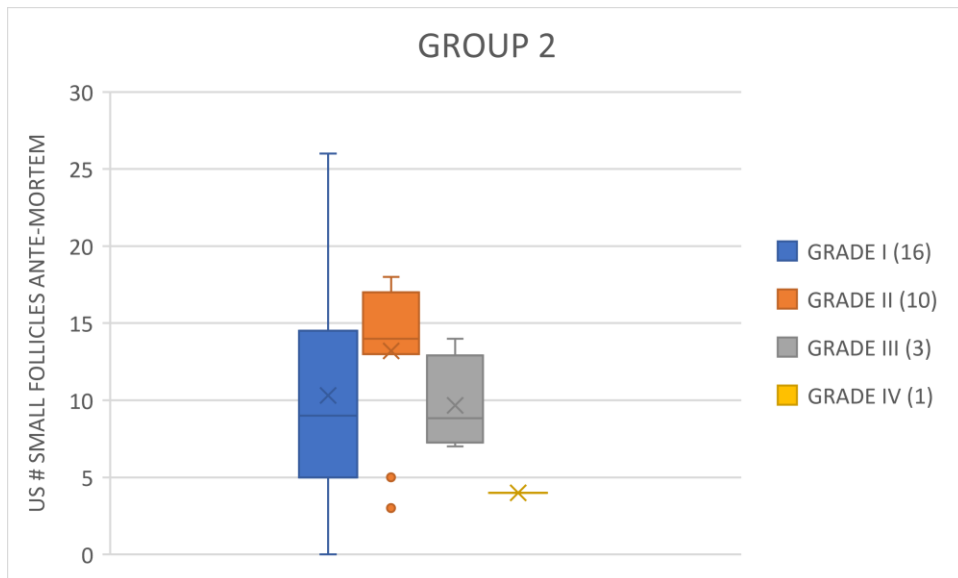
Appendix 12 - Graph illustrating the number of post-mortem antral follicle count (AFC) in ovaries with US OFD grades III and IV from group 1.



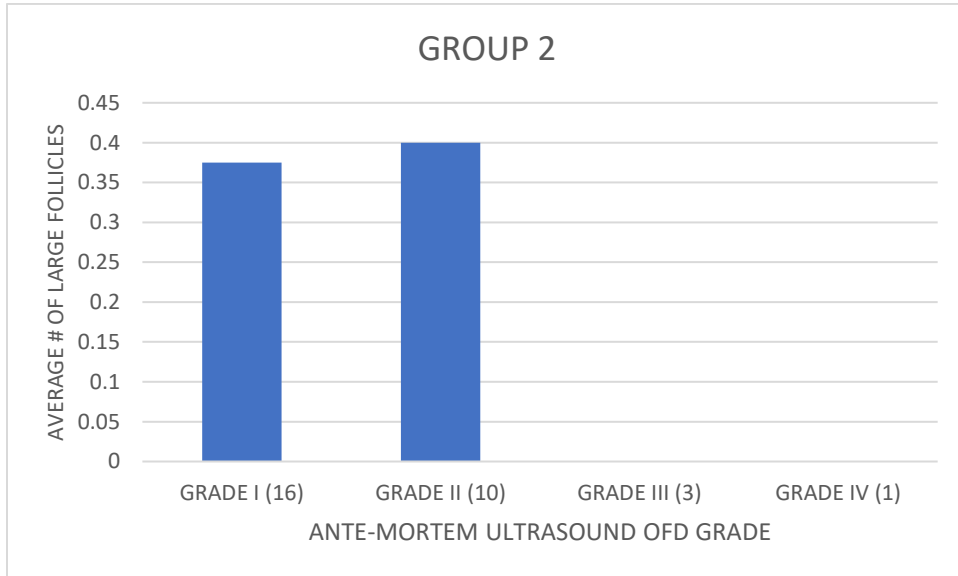
Appendix 13 - Graph illustrating the average of ante-mortem antral follicle count (AFC) number of small follicles (<4mm) in ovaries with US OFD grades I, II, III and IV from group 2.



Appendix 14 - Graph illustrating the ante-mortem antral follicle count (AFC) numbers of small follicles (<4mm) in ovaries with US OFD grades I, II, III and IV from group 2.



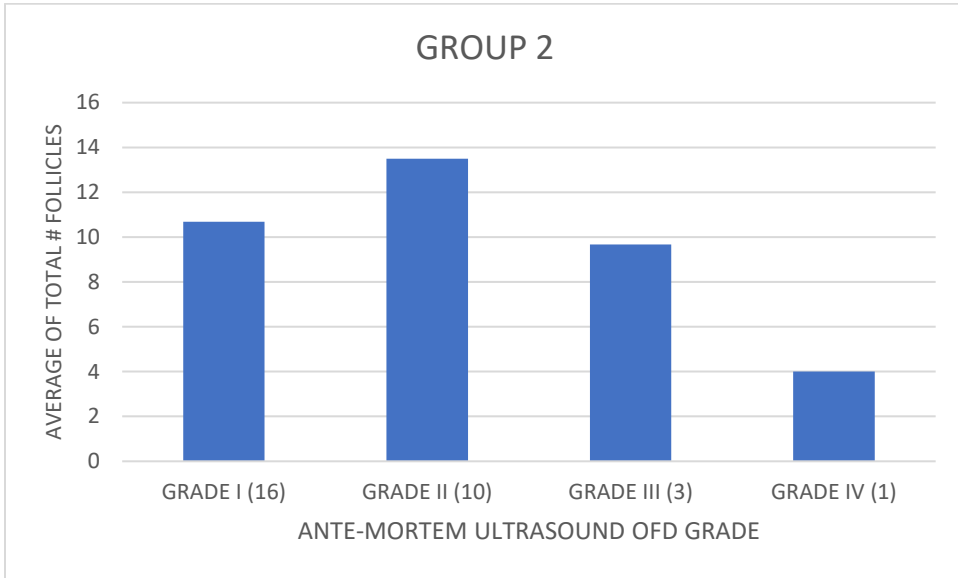
Appendix 15 - Graph illustrating the average of ante-mortem antral follicle count (AFC) numbers of large follicles ($\geq 5\text{mm}$) in ovaries with US OFD grades I, II, III and IV from group 2.



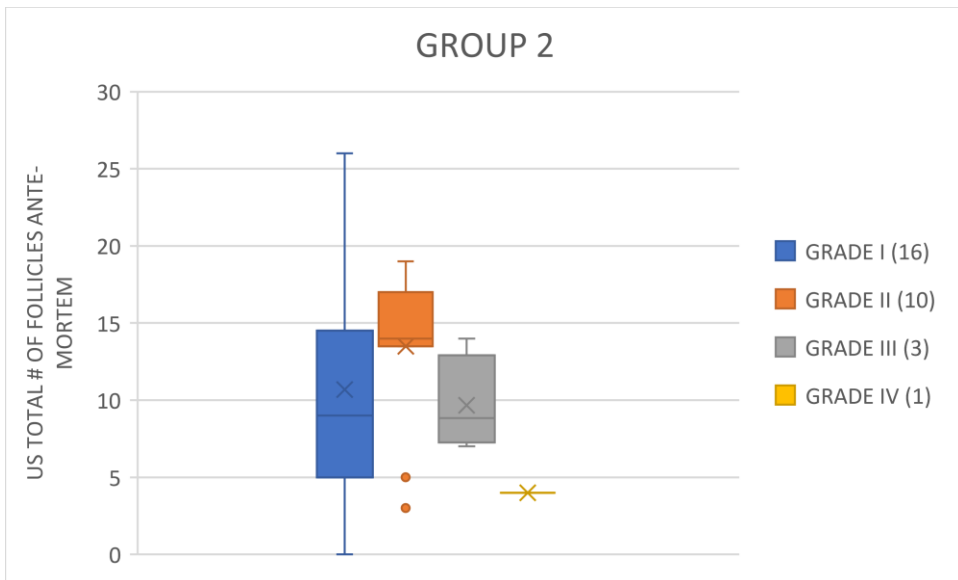
Appendix 16 - Graph illustrating the ante-mortem antral follicle count (AFC) numbers of large follicles ($\geq 5\text{mm}$) in ovaries with US OFD grades I, II, III and IV from group 2.



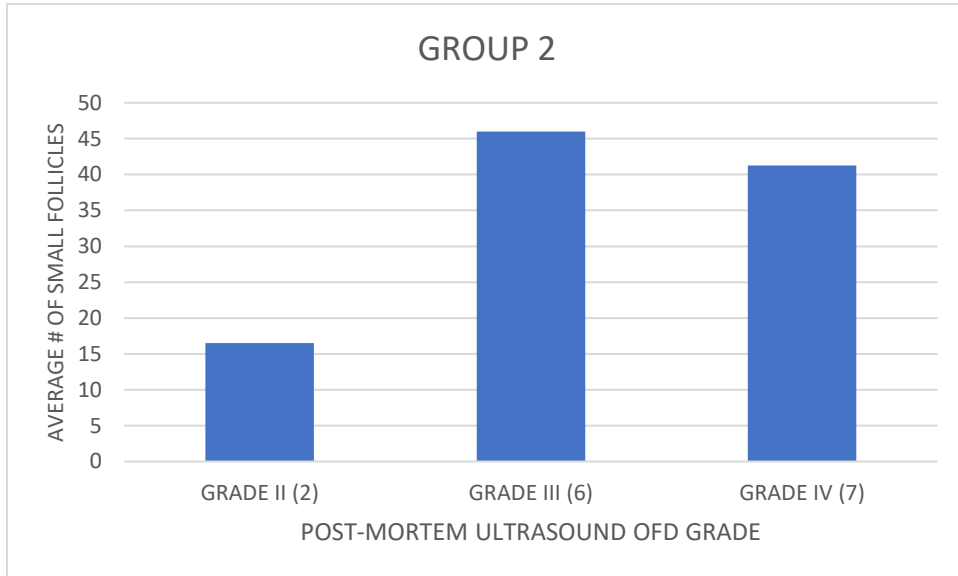
Appendix 17 - Graph illustrating the average number of ante-mortem antral follicle count (AFC) in ovaries with US OFD grades I, II, III and IV from group 2.



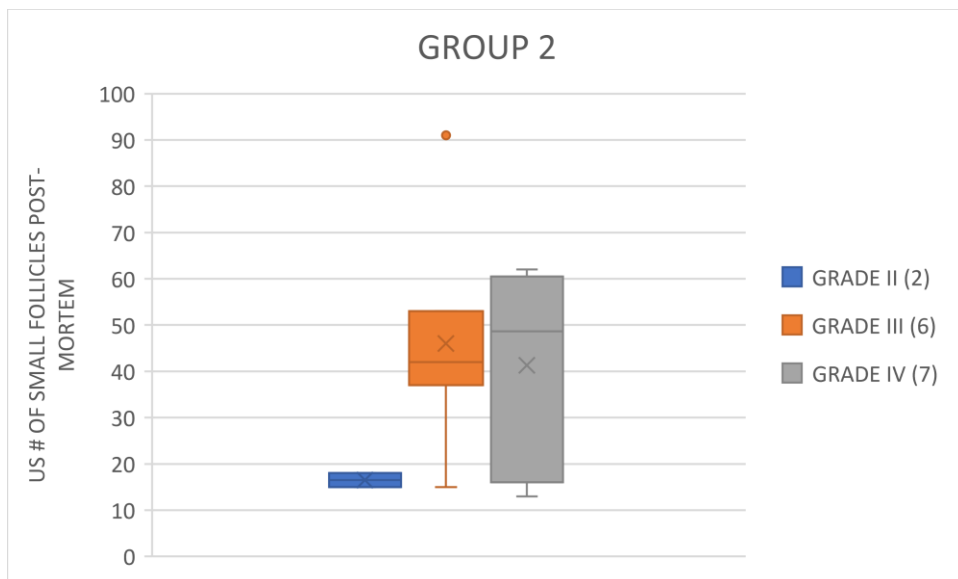
Appendix 18 - Graph illustrating the number of ante-mortem antral follicle count (AFC) in ovaries with US OFD grades I, II, III and IV from group 2.



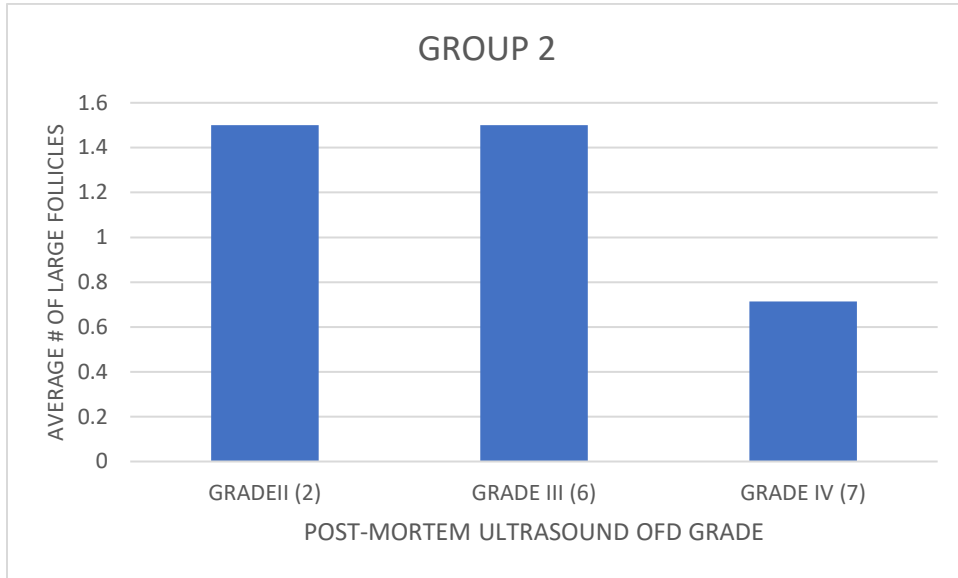
Appendix 19 - Graph illustrating the average of post-mortem antral follicle count (AFC) numbers of small follicles (<4mm) in ovaries with US OFD grades II, III and IV from group 2.



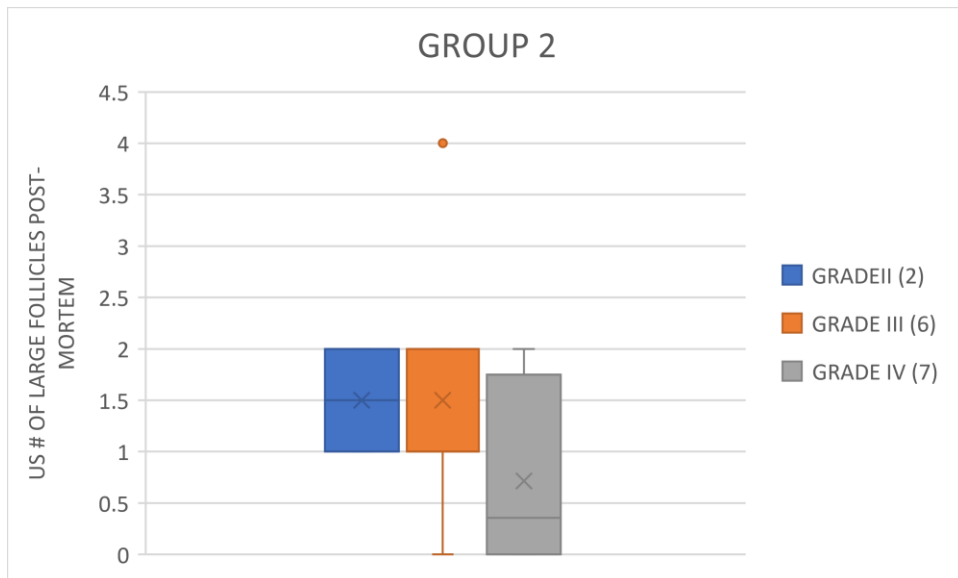
Appendix 20 - Graph illustrating the numbers of post-mortem antral follicle count (AFC) numbers of small follicles (<4mm) in ovaries with US OFD grades II, III and IV from group 2.



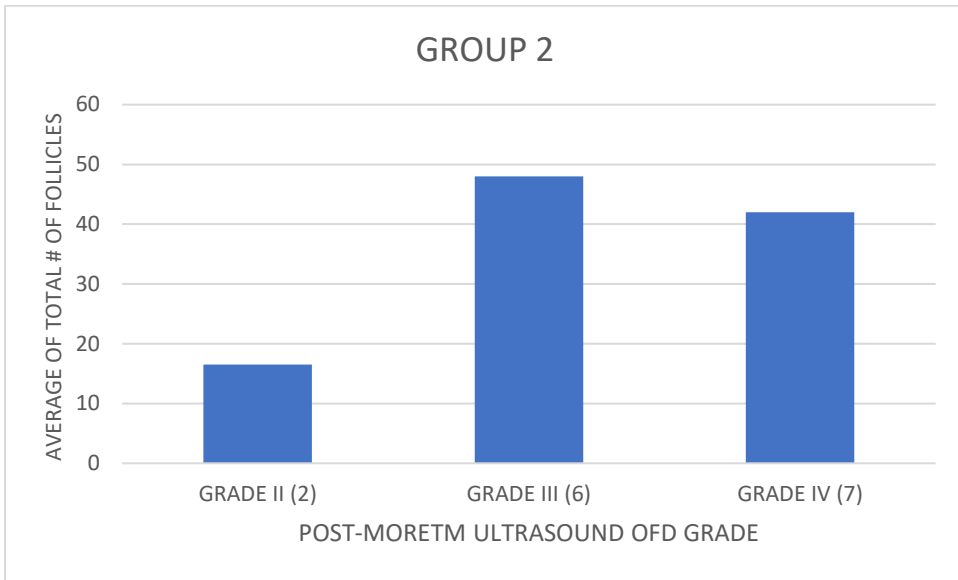
Appendix 21 - Graph illustrating the average of post-mortem antral follicle count (AFC) numbers of large follicles ($\geq 5\text{mm}$) in ovaries with US OFD grades II, III and IV from group 2.



Appendix 22 - Graph illustrating the post-mortem antral follicle count (AFC) numbers of large follicles ($\geq 5\text{mm}$) in ovaries with US OFD grades II, III and IV from group 2.



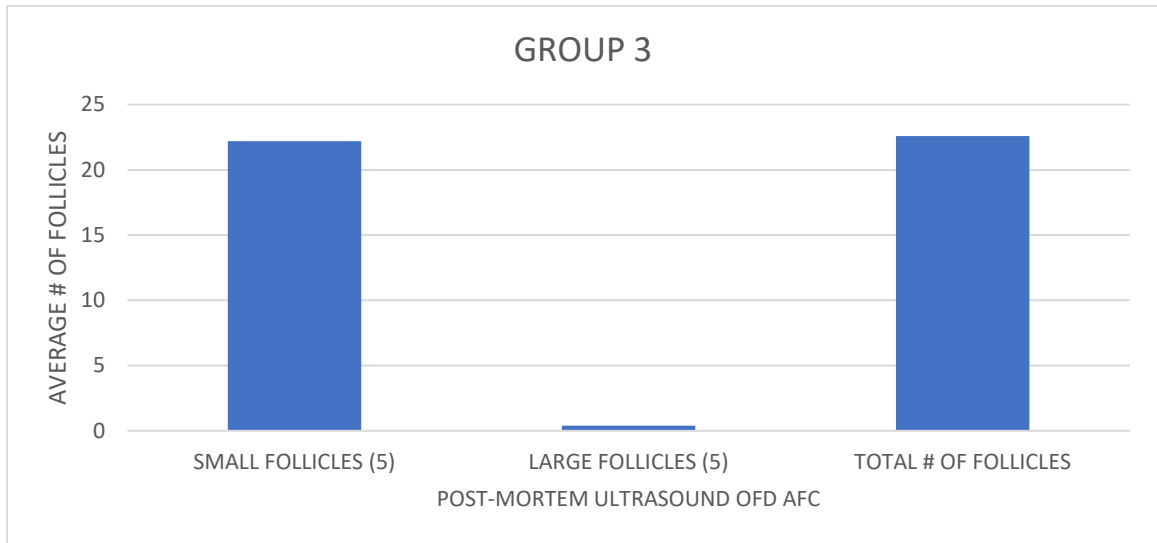
Appendix 23 - Graph illustrating the average number of post-mortem antral follicle count (AFC) in ovaries with US OFD grades II, III and IV from group 2.



Appendix 24 - Graph illustrating the number of post-mortem antral follicle count (AFC) in ovaries with US OFD grades II, III and IV from group 2.



Appendix 25 - Graph illustrating the average number of post-mortem antral follicle count (AFC) in ovaries with US OFD grade I from group 3.



Appendix 26 – Ante-mortem US, Post-mortem US and Histology data for Group 1.

COWID	L/R	ASmF	ALgF	ACL-HEch	ACL+HEch	AHEch	PSmF	PLgF	PCL-HEch	PCL+HEch	PHEch	AOFD	POFD	HOFD	P/O
101	L	4	1	0	0	2 (15)	37	1	0	0	6 (51-60)	1	3	1	O
101	R	7	0	0	1	2 (18)						1		1	
102	L	5	1	0	0	1 (8)						1		0	O
102	R	3	1	1	0	2 (11)	48	1	1	0	7 (61-70)	1	4	0	
103	L	11	1	0	0	1 (9)						1		1	O
103	R	6	0	1	0	2 (13)	51	0	0	1	8 (71-80)	1	4	1	
104	L	6	0	0	0	3 (21)						2		0	P
104	R	11	0	0	1	2 (16)						1		0	
105	L	13	0	0	0	3 (29)						2		0	O
105	R	11	0	0	1	5 (41)						3		0	
106	L	9	0	0	0	3 (22)						2		1	O
106	R	8	1	0	1	3 (25)	36	1	0	1	10 (TNC)	2	4	1	
107	L	15	0	0	0	2 (12)	54	0	0	0	8 (71-80)	1	4	0	O
107	R	25	1	0	0	4 (33)						2		0	
108	L	23	0	0	0	2 (18)						1		0	O
108	R	7	2	0	0	4 (32)						2		0	
109	L	16	0	0	1	3 (28)						2		1	P
109	R	25	0	0	0	2 (18)						1		1	
110	L	22	0	0	0	4 (37)						2		1	O
110	R	33	0	0	0	5 (45)	68	1	0	1	10 (TNC)	3	4	1	
111	L	29	0	0	0	3 (24)	41	0	0	0	7 (61-70)	2	4	1	O
111	R	16	0	0	0	3 (26)						2		1	
112	L	24	0	0	0	3 (23)						2		1	O
112	R	28	0	0	0	3 (27)	87	1	0	0	9 (81-90)	2	4	1	
113	L	16	0	0	0	3 (21)						2		1	O
113	R	12	1 (H)	0	0	2 (20)	53	1 (H)	0	0	10 (TNC)	1	4	1	
114	L	8	0	0	0	2 (17)	15	0	0	1	10 (TNC)	1	4	1	P
114	R	13	0	0	0	3 (23)						2		1	
115	L	15	1	1	0	3 (26)						2		1	O
115	R	11	0	0	0	4 (31)						2		0	

COWID = Cow Identification

Table of Abbreviations and Scores	
L/R = Left or Right ovary	
ASmF = Ante-mortem Small Follicles (SmF<4mm)	
ALgF = Ante-mortem Large Follicles (LgF ≥5mm)	
ACL-HEch = Ante-mortem CL without hyperechogenicity	
ACL+HEch = Ante-mortem CL with hyperechogenicity	
AHEch = Ante-mortem hyperechogenicity score	
PSmF = Post-mortem Small Follicles (SmF<4mm)	
PLgF = Post-mortem Large Follicles (LgF ≥5mm)	
PCL-HEch = Post-mortem CL without hyperechogenicity	
PCL+HEch = Post-mortem CL with hyperechogenicity	
PHEch = Post-mortem hyperechogenicity score	
P/O = Pregnant or Open	
HOFD = Histologic OFD grade	
TNC = Too numerous to count	
HEch = Hyperechogenicity	
Hyperechogenicity Score	
0 = Normal	
1 = 1 - 10	
2 = 11 - 20	
3 = 21 - 30	
4 = 31 - 40	
5 = 41 - 50	
6 = 51 - 60	
7 = 61 - 70	
8 = 71 - 80	
9 = 81 - 90	
10 = ≥ 91 (TNC)	
OFD Score	
0 = Normal	
1 = 1 - 2 Hech	
2 = 3 - 4 Hech	
3 = 5 - 6 Hech	
4 = ≥ 6 Hech	

APPENDIX 27 - Ante-mortem US, Post-mortem US and Histology data for Group 2.

COWID	L/R	ASmF	ALgF	ACL-HEch	ACL+HEch	AHEch	PSmF	PLgF	PCL-HEch	PCL+HEch	PHEch	AOFD	POFD	HOFD	P/O
1S	L	10	1	0	1	1 (10)	TNC	4	0	0	5 (41-50)	1	3	1	O
1S	R	20	2	0	0	2 (12)						1		1	
2S	L	8	1	0	0	2 (18)						1		1	O
2S	R	5	0	0	0	2 (11)	53	0	0	0	5 (41-50)	1	3	1	
3S	L	16	1	0	0	3 (27)						2		3	O
3S	R	18	1	0	0	3 (28)	37	1	0	0	6 (51-60)	2	3	3	
4S	L	9	0	0	0	2 (14)						1		1	O
4S	R	16	0	0	0	1 (8)	61	1	0	1	7 (71-80)	1	4	1	
5S	L	13	1	0	0	4 (33)						2		2	O
5S	R	14	0	0	0	3 (22)	59	2	0	0	TNC	2	4	2	
6S	L	18	0	0	0	3 (21)						2		1	O
56	R	26	0	0	0	2 (16)	62	0	0	0	9 (81-90)	1	4	1	
7S	L	8	0	0	0	2 (14)						1		2	O
7S	R	14	0	0	0	3 (25)	25	2	0	0	7 (61-70)	2	4	2	
8S	L	3	0	1	0	3 (27)	13	0	0	1	TNC	2	4	2	O
8S	R	5	0	0	0	3 (21)						2		2	
9S	L	13	0	1	0	2 (20)						1		2	O
9S	R	8	0	0	0	5 (43)	15	1	0	0	5 (41-50)	3	3	2	
10S	L	18	0	0	0	2 (11)						1		1	O
10S	R	8	0	0	0	2 (18)	42	1	1	0	5 (41-50)	1	3	1	
11S	L	7	0	0	1	5 (47)	13	0	0	1	TNC	3	4	3	P
11S	R	4	0	0	0	7 (62)						4		3	
12S	L	17	0	0	0	3 (26)						2		1	O
12S	R	14	0	1	0	5 (47)	56	0	0	1	7 (61-70)	3	4	2	
13S	L	4	1	0	0	1 (8)	15	1	0	0	4 (31-40)	1	2	0	P
13S	R	0	0	0	1	2 (17)						1		0	
14S	L	14	0	0	0	3 (21)						2		1	O
14S	R	11	1	0	0	2 (19)	38	2	1	0	6 (51-60)	1	3	1	
15S	L	5	0	0	0	1 (9)						1		1	O
15S	R	4	0	1	0	2 (19)	18	2	1	0	4 (31-40)	1	2	1	

COWID = Cow Identification

Table of Abbreviations and Scores

L/R = Left or Right ovary
ASmF = Ante-mortem Small Follicles (SmF<4mm)
ALgF = Ante-mortem Large Follicles (LgF ≥5mm)
ACL-HEch = Ante-mortem CL without hyperechogenicity
ACL+HEch = Ante-mortem CL with hyperechogenicity
AHEch = Ante-mortem hyperechogenicity score
PSmF = Post-mortem Small Follicles (SmF<4mm)
PLgF = Post-mortem Large Follicles (LgF ≥5mm)
PCL-HEch = Post-mortem CL without hyperechogenicity
PCL+HEch = Post-mortem CL with hyperechogenicity
PHEch = Post-mortem hyperechogenicity score
P/O = Pregnant or Open
HOFD = Histologic OFD grade
TNC = Too numerous to count
HEch = Hyperechogenicity

Hyperechogenicity Score

0 = Normal
1 = 1 - 10
2 = 11 - 20
3 = 21 - 30
4 = 31 - 40
5 = 41 - 50
6 = 51 - 60
7 = 61 - 70
8 = 71 - 80
9 = 81 - 90
10 = ≥ 91 (TNC)

OFD Score

0 = Normal
1 = 1 - 2 Hech
2 = 3 - 4 Hech
3 = 5 - 6 Hech
4 = ≥ 6 Hech

